# BIOPRINTING OF PANCREATIC CANCER CELLS FOR IMPROVED DRUG TESTING

A Thesis
Submitted to the Graduate Faculty
of the
North Dakota State University
of Agriculture and Applied Science

By

Chad Austin Rehovsky

In Partial Fulfillment of the Requirements
for the Degree of
MASTER OF SCIENCE

Major Department:
Mechanical Engineering

May 2019

Fargo, North Dakota

# North Dakota State University
Graduate School

**Title**

BIOPRINTING OF PANCREATIC CANCER CELLS FOR IMPROVED DRUG TESTING

**By**

Chad Austin Rehovsky

The Supervisory Committee certifies that this ***disquisition*** complies with North Dakota State University's regulations and meets the accepted standards for the degree of

**MASTER OF SCIENCE**

SUPERVISORY COMMITTEE:

Dr. Dilpreet Bajwa
Chair

Dr. Sanku Mallik

Dr. Jordi Estevadeordal

Approved:

June 4, 2019
Date

Dr. Alan Kallmeyer
Department Chair

## ABSTRACT

Currently, many drugs are preclinically tested on two-dimensional cell cultures. However, this method does not adequately replicate the cellular interactions or diffusion gradient that occur in three-dimensional tissues, leading to poor indicators of how a drug may affect human tissues. The objective of this project was to use bioprinted pancreatic cancer cell cultures as a platform for three-dimensional drug testing. Various bioink formulations of cellulose, gelatin, and alginate were evaluated to determine which provided the best printability and cell viability. A cellulose nanocrystal and alginate hydrogel showed superior printability due to its shear thinning properties. Additionally, initial cell viability was nearly 80%, and it remained above 60% over four days. Use of a custom spinning bioreactor at 50 rpm resulted in no improvements to cell viability. Overall, the system shows potential as a drug testing platform to evaluate the effectiveness of various drug formulations on three-dimensional pancreatic cancer cell cultures.

## ACKNOWLEDGEMENTS

I would like to firstly thank my advisors Dr. Dilpreet Bajwa and Dr. Sanku Mallik. They provided me with the opportunity to continue my education while exploring the biomedical field. Their guidance and flexibility allowed me to find a project that I truly enjoyed and to expand my education to areas I never would have imagined when I started. They helped me push my boundaries and made me a better researcher and person. I would also like to thank my committee member, Dr. Jordi Estevadeordal, for always being available and willing to help when I came to him with questions.

I would like to acknowledge all my fellow graduate students who have helped me during my time at NDSU. Specifically, I would like to thank Jamileh Shojaeiarani for all her help improving the technical aspects of my writing, and Jessica Pullan, Matthew Confeld, and Babak Mamnoon for their help and patience with me as I learned the basics of cell culture.

Lastly, I would like to thank Dr. Amanda Brooks for allowing me to use her lab and Dr. Pawel Borowicz from the NDSU AIM laboratory for his help and expertise in the imaging of my hydrogel. I am grateful for the financial support of the NIH (Grant 1R01 GM114080), North Dakota Industrial Commission, and U.S. Forests Products Laboratory.

## TABLE OF CONTENTS

## LIST OF TABLES

## LIST OF FIGURES

## LIST OF ABBREVIATIONS

Al.....Alginate.

ATCC.....American Type Culture Collection.

$CaCl_2$.....Calcium Chloride.

CAD.....Computer Aided Design.

CF.....CelluForce.

CMC.....Carboxymethyl Cellulose.

CNCs.....Cellulose Nanocrystals.

CNFs.....Cellulose Nanofibers.

CT.....Computerized Tomography.

DMEM.....Dulbecco's Modified Eagle Media.

FBS.....Fetal Bovine Serum.

FPL.....Forest Products Lab.

Gel.....Gelatin.

LAB.....Laser Assisted Bioprinting.

LVR.....Linear Viscoelastic Region.

MRI.....Magnetic Resonance Imaging.

NIH.....National Institutes of Health.

PBS.....Phosphate Buffered Saline.

PEG.....Polyethylene Glycol.

STL.....Stereolithography.

## LIST OF SYMBOLS

°C .....Degrees Celsius.

G.....Gauge.

G*.....Complex Modulus.

G’ .....Storage Modulus.

G”.....Loss Modulus.

Hz.....Hertz.

K.....Fluid Consistency.

kPa.....Kilopascal.

mL.....Milliliter.

mM.....Millimolar.

mm .....Millimeter.

mm/s.....Millimeters per Second.

n.....Flow Behavior Index.

nm .....Nanometer.

η .....Apparent Viscosity.

Pa.....Pascal.

Pa·s.....Pascal Second.

psi.....Pounds per Square Inch.

Q.....Volumetric Flow Rate.

r .....Radius.

rpm .....Revolutions per Minute.

$s^{-1}$.....Per Second.

µL.....Microliter.

µL/s .....Microliters per Second.

µM.....Micromolar.

µm .....Micrometer.

V.....Volts.

w/v% .....Weight/Volume Percent.

$\dot{\gamma}$ .....Shear Rate.

# 1. INTRODUCTION

## 1.1. Motivation

Cancer accounted for an estimated 9.6 million deaths worldwide in 2018, and with another 18.1 million new diagnoses in the same year, the need for new treatments and therapies is as great as ever [1]. However, only about 1 in 15 drugs that make it to clinical trials in the oncology field will actually end up being approved by the Food and Drug Administration [2]. This highlights the need for better drug screening tools at the preclinical level.

Currently, most drugs are tested on two-dimensional monolayer cell cultures before moving onto animal trials. Two-dimension cultures grown in multi-well plates or Petri dishes allow for controlled, rapid testing while still maintaining a low overall cost. Animal models, on the other hand, better replicate the complex nature of human tissues and organs [3]. Although both methods are important and useful, they also have obvious shortcomings. Two-dimensional cultures do not show the cell to cell interactions and complex tissues architectures that are found in vivo [3]. Also, the hard growing surface is much different than the natural extracellular matrix found in the body, which plays a role in cell differentiation, growth, migration, and homeostasis [4], and research has shown that drug sensitivity and toxicity vary between two and three-dimensional cell cultures [5]. Compared to two-dimensional cultures, animal models are much more costly and more limited in availability, and even though they are an in vivo model, toxicity results may not translate well from animals to humans because of the difference in species. Additionally, ethical concerns are creating a growing push to reduce the use of animals in preclinical testing [6].

Because of these issues, there has been an increased use of three-dimensional in vitro models for cancer drug development as they allow for the testing of human cells in more realistic

three-dimensional architectures. This three-dimensional structure is crucial because it has been shown that both composition and architecture play important roles in cellular behavior [7]. Thus, by better mimicking the in vivo environment using these three-dimensional models, more accurate information about toxicity and cellular responses can be obtained earlier in the drug development process. Figure 1 illustrates how three-dimensional models can be implemented to help reduce the number of animal trials and increase the success rates of clinical trials. Currently used three-dimensional culture models include spheroids, microfluidics, and scaffolds [6].

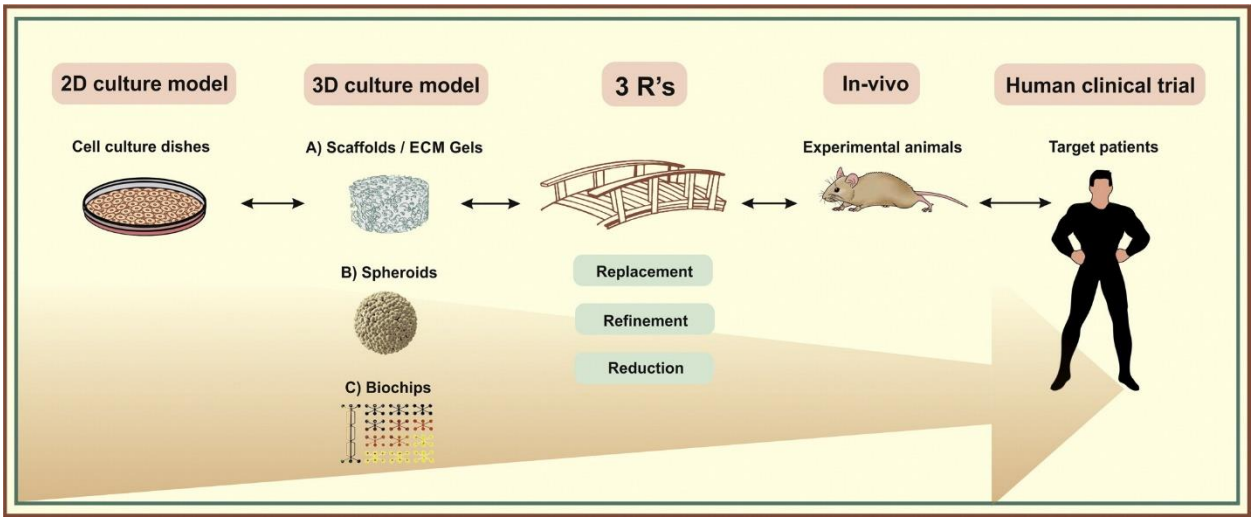


Figure 1. Schematic of models used in drug development showing how three-dimensional culture models can be used to help reduce animal trials and improve clinical trial success rates. Reprinted from [6] with permission from Elsevier.

Spheroids are heterogeneous cell aggregates that have a necrotic core similar to that of a tumor [8]. Because of their close similarity to a tumor microenvironment as well as their reproducibility and well-defined geometry, they are commonly used in drug development studies. However, they are not compatible with all cell types, and they may form undesired shapes [9].

Microfluidics consist of small cell cultures on miniature chips that are connected to fluidic systems [10]. This type of system better mimics the shear forces and diffusion of nutrients

that occurs in vivo [11]. Additionally, they allow for a lower number of cells and a smaller amount of drug to be tested compared to many other models [12]. Because of the unique setup and minimized size though, microfluidics require fairly complex equipment and the development of specialized protocols to run the systems [13].

Scaffolds are artificial three-dimensional structures that provide a matrix for cells to grow and proliferate in. They can be manufactured using either a two-step or one-step biofabrication process. In two-step biofabrication, the scaffold is produced and then seeded with cells; while in one-step biofabrication, the cells are premixed with the scaffold material before fabrication. The advantage of one-step biofabrication is better repeatability in terms of cell densities and scaffold dimensionality [14].

Advantages of three-dimensional scaffold models over traditional two-dimensional models include improved control over the mechanical, biological, and biochemical properties of the cellular environment. By optimizing these properties, cells are more likely form into tumor-like spheroids with more realistic protein and gene expressions [15, 16]. These factors affect cell viability [17], proliferation [18], migration [19], organization [17], morphology [17], and most important for this application, drug response [20-27]. Cells in two-dimensional cultures tend to show stronger responses to drugs than those in three-dimensional ones. Potential explanations to this include a lower rate of diffusion in the three-dimensional cultures as well as increases in the expression of drug resistance proteins [22]. It has even been reported that some three-dimensional cultures are resistant to certain anti-cancer drugs even when the same treatment is effective on two-dimensional cultures of the same cell type [23].

Overall, it has been determined that the chemosensitivity of cancer cells is affected by both the specific drug and cell line used [24]. As an example, PANC-1 pancreatic cancer cells

cultured in a fibroblast derived matrix showed a higher resistance to the drug paclitaxel compared to cells cultured in traditional two-dimensional cultures. However, when four other drugs were tested on the PANC-1 cells, similar drug sensitivities were observed between two-dimensional cultures and those cultured in the fibroblast derived matrix [25]. Three-dimensional models have also allowed for the testing of cell lines that have poor adherence in two-dimensional cultures. For example, LNCaP prostate cancer cells were cultured in a hyaluronic acid hydrogel, which eliminated the adherence issues and allowed for better drug sensitivity testing [27]. In addition to traditional drug development, these three-dimensional models can be used to study drug carriers and targeted treatment options. In a recent study, free doxorubicin and polymer-nanoparticle encapsulated doxorubicin were tested on LNCaP cells in hydrogel cultures. It was shown that the three-dimensional cultures were more resistant to both the free and encapsulated drugs and that the nanoparticle uptake mechanism differed between the different culture methods [22].

Various methods of scaffold manufacturing have been studied including but not limited to electrospinning [26], freeze drying [28, 29], gas foaming [30], and particle leaching [30], but arguably the most exciting new method is the additive manufacturing technique of three-dimensional bioprinting. Figure 2 illustrates different scaffold preparation techniques as well as their resulting microscopic structures [31]. The three-dimensional porous structure that can be created by these methods provides the required mechanical integrity while still allowing oxygen, nutrients, and waste to move freely. Typical pore sizes range from micrometer to nanometer scale and are dependent on the manufacturing process.

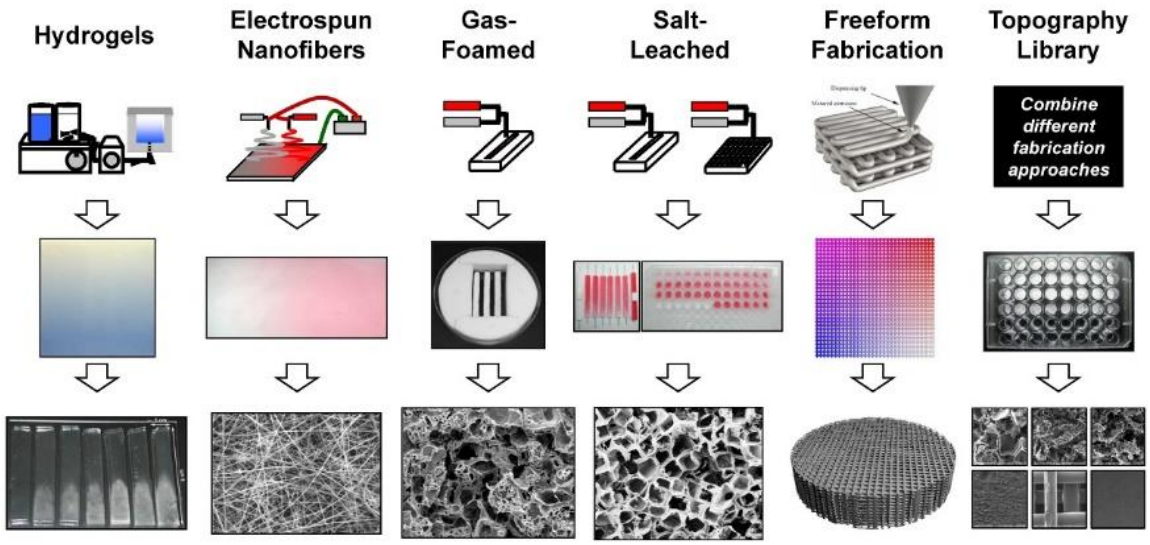


Figure 2. Various methods of scaffold preparation used for cell culture applications along with their resulting structures. These three-dimensional porous structures provide the necessary mechanical properties while also providing space for cell to grow and small molecules to diffuse freely. Reproduced from [31].

Three-dimensional bioprinting is an additive manufacturing technique where cells embedded in a biomaterial are deposited layer by layer to construct a three-dimensional structure. It is an easily customizable process that allows for rapid production of complexly shaped scaffolds while providing accurate reproducibility [14]. Bioprinting allows for the printing of multiple materials, which is useful when trying to replicate in vivo structures. Different cell types, extracellular matrix components, and biomolecules can be spatially arranged to mimic complex tumor microenvironments [32]. In one study, HeLa cervical cancer cells were encapsulated in a gelatin, alginate, and fibrinogen hydrogel and bioprinted to create an in vitro cervical tumor model. Compared to two-dimensional cultures, it was found that the bioprinted cultures tended to show greater cell proliferation and form cellular spheroids while also displaying higher protein expressions and drug resistance [21]. Studies like this emphasized the need from the continued development of three-dimensional bioprinted cell culture models for drug development and testing.

## 1.2. Objectives and Hypothesis

Because of the advantages of three-dimensional cell culture models for drug development compared to traditional two-dimensional models, the overall goal of this research was to develop a system for rapid, accurate drug testing of bioprinted pancreatic cancer cell cultures. To achieve this, the following three objectives and hypotheses were developed.

The first objective was to formulate a hydrogel bioink with good printability, shape fidelity, and biocompatibility. It was hypothesized that a cellulose and alginate bioink would provide the required shape fidelity and printability as well as good biocompatibility.

The second objective was to design a spinning bioreactor to improve the ease and effectiveness of drug testing. It was hypothesized that media circulation would improve cell viability and drug dispersion. Additionally, a speed controller would allow for adjustments to the rotational speed, and drug inlet ports would allow for easy deposition of drug formulations into the wells of the plate.

The third objective was to bioprint three-dimensional scaffolds containing pancreatic cancer cells to improve the accuracy of drug testing. It was hypothesized that bioprinted cell cultures would better replicate in vivo conditions compared to traditional methods by better matching the cellular interactions and diffusion gradient.

## 2. LITERATURE REVIEW

A major topic in today's healthcare is the shortage of donor organs and tissues as there are over 114,000 people on the transplant list in the Unites States alone [33]. Strides are being made within the biomedical community to develop new approaches to overcome failure within organs and tissues. Tissue engineering by method of three-dimensional bioprinting has become a new and effective tool to construct new organs and tissues that are compatible with the human body. Bioprinting is an additive manufacturing technique where cells encapsulated in a biomaterial are deposited layer by layer into a three-dimensional structure [34]. Recently, it has received much attention due to rapid innovations in printer and biomaterial technology.

The bioprinting process begins by constructing a computer aided design (CAD) model in the shape of interest. This can be accomplished by either creating a custom model or uploading a magnetic resonance imaging (MRI) or computerized tomography (CT) scan of the organ or tissue of interest [34-36]. Then a slicing program is used to convert the STL file of the model into G-code, which can control the movements of the bioprinter. Many slicing programs, however, are designed for use with 3-D printers as opposed to bioprinters, so the setting must be adjusted to account for the differences in printer functionality and material characteristics.

After the G-code is prepared, a mixture of the chosen biomaterial and cell type is inserted into the bioprinter and deposited onto the print bed into the desired three-dimensional structure. Lastly, the structure may be cross-linked before it is placed in an incubator, where the cells are allowed to grow and proliferate [35]. Figure 3 illustrates the steps in the bioprinting process.

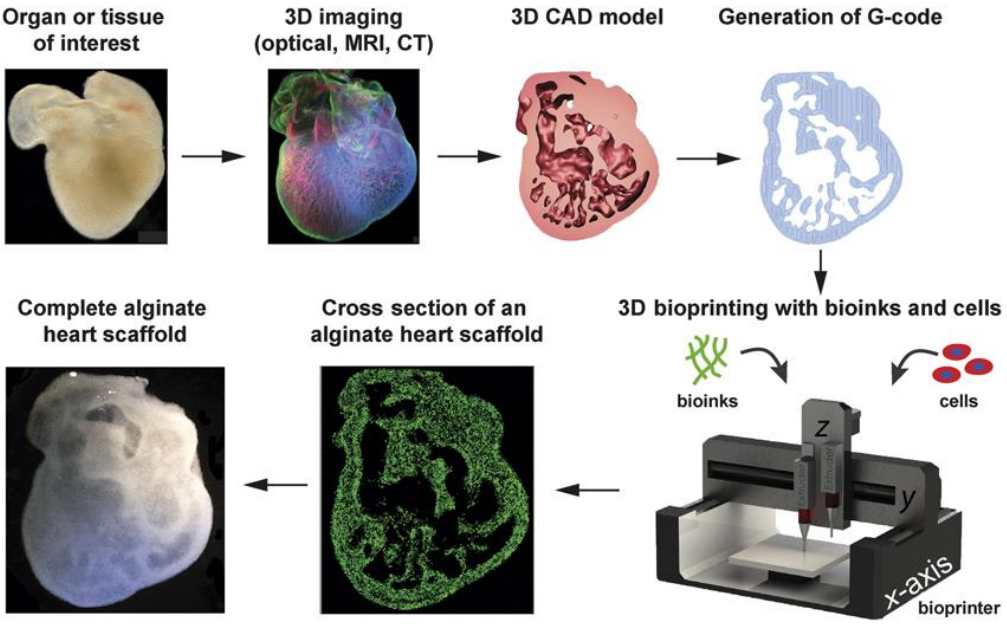


Figure 3. Schematic of the bioprinting process from tissue selection through manufacturing of three-dimensional tissues. [36], reproduced with permission.

### 2.1. Methods of Bioprinting

In today's engineering community, there are four major approaches to three-dimensional bioprinting (Figure 4): inkjet, stereolithography, laser assisted, and extrusion [36-38]. Each method involves different processing conditions that lead to both advantages and disadvantages.

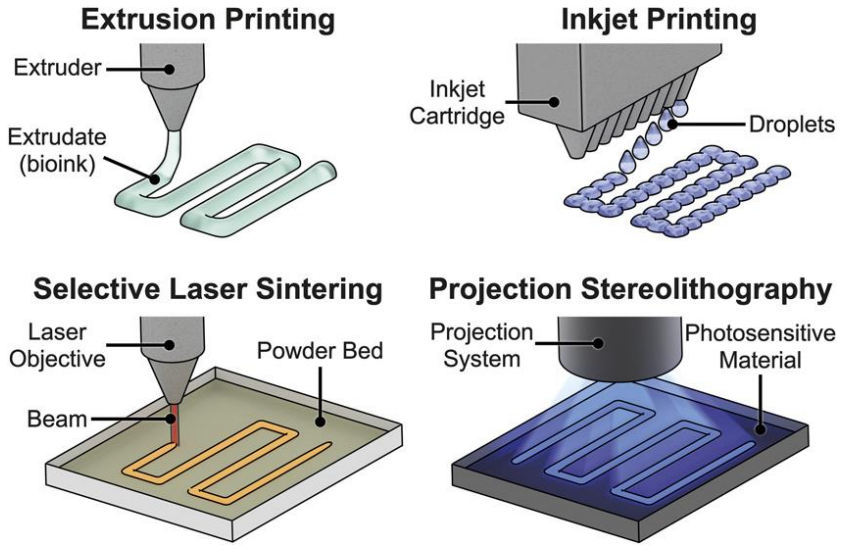


Figure 4. Illustrations of material deposition techniques for common bioprinting methods. [36], reproduced with permission.

Inkjet bioprinting is a non-contact printing process where picoliter droplets of biomaterial are deposited onto a print bed similar to traditional desktop printers [38]. These droplets can be generated using thermal and piezoelectric processes [38]. Inkjet printing is relatively affordable, and the equipment required is easily available [37]. The process though can expose cells to thermal and mechanical stresses causing cell membrane damage or cell lysis [39], and it sometimes has poor cell encapsulation [37]. Additionally, inkjet biomaterials are generally very soft making them sometimes unable to withstand normal physiological conditions [38].

Stereolithography (STL) uses illumination to solidify a liquid, photo-sensitive polymer [38]. It offers high fabrication accuracy and allows for many different biomaterials to be used [38]. However, only one biomaterial type may be used at a time [40], and it can only print single cell types [37]. Additionally, the photocuring process and residual photocuring reagents can cause harmful effects to the cells [38].

Laser assisted bioprinting (LAB) uses the energy from a laser to evaporate a biomaterial containing cells off a ribbon. The droplet that is formed then lands on a receiving substrate where the cells can adhere and growth [38]. When compared with other bioprinting techniques, LAB offers advantages such as a nozzle free printing and high print resolution [38]. Conversely, it requires more expensive equipment that is less readily available [37].

Extrusion or pressure assisted bioprinting uses pneumatic pressure, a piston, or a screw to force a biomaterial through a nozzle onto a stationary surface [35]. One advantage of extrusion bioprinting is that the syringe, nozzle, and bed of the printer can all be heated to physiological conditions to help ensure good cell viability [41]. Cells are directly incorporated and distributed in the biomaterial, which allows for high cell densities in the print [37]. However, the shear forces applied to the cells during printing, which are influenced by the print pressure and nozzle

size, can negatively affect cell viability. It has been reported that pressure plays a larger role in determining the shear stresses on cells, as nearly a 40% decrease in cell viability was observed when print pressure was increased from 5 psi to 40 psi [42]. This research focused on the application of extrusion bioprinting.

### 2.2. Material Properties Required for Extrusion Bioprinting

Biomaterials used for bioprinting are commonly termed bioinks, and they can come from both natural and synthetic origins. When choosing a bioink for extrusion bioprinting, a variety of properties need to be considered. Often, a balance between the structural and physiological properties of the material must be found [34, 41]. The bioink needs to support cell growth and development while still providing the dimensional stability required to mimic the structure of complex heterogeneous tissues. Key factors in choosing a bioink material include printability, shape fidelity, and support of cell viability and functionality [41]. Ideally, the stiffness of the material should match that of the natural tissues as matrix stiffness has been shown to play a role in cell geometry and differentiation [43]. The viscosity of the bioink also plays a key role as the material needs to flow through a small nozzle yet hold its shape after it has been deposited on the print bed. Bioinks with shear thinning properties are desirable because they are able to display higher viscosities at lower shear rates and conversely lower viscosities at higher shear rates. In extrusion bioprinting, these high shear rates occur when the material is forced through the nozzle, which aligns the polymer chains and allow the material to flow. Then when the material is deposited on the print bed, the shear rate is dramatically reduced, and the material can solidify to maintain its desired shape [34, 35, 41]. The bioink should also have low adhesion and surface tension to prevent curling at the tip of the nozzle, and rapid gelation to prevent spreading on the extrusion bed [34]. In terms of cellular compatibility, bioinks should have cell binding domains

to facilitate adherence, and they should promote cellular proliferation, spreading, communication, and differentiation so that structures can develop into functional tissues [34, 41, 44].

To achieve a combination of the most desirable properties, materials may be chemically altered, or various material types may be blended together. However, there is still a need to develop bioinks that better meet the requirements of functional organ bioprinting. To print transplantable organs, bioinks must be developed that degrade at a rate similar to that of new tissue formation [34]. This will allow structures to retain their desired shape yet allow cells to expand and eventually replace the bioink with their own extracellular matrix. The rate of degradation will vary between in vivo and in vitro as tissues are exposed to various enzymes, immune responses, and blood flow in vivo [34]. Different bioinks are necessary for each cell type as each tissue has a unique set of mechanical properties and also will require different functional cues including binding sites and specific growth factors [41].

### 2.3. Materials Commonly Used for Extrusion Bioprinting

Hydrogels are a common material type used in extrusion bioprinting, and they typically consist of a small percentage of polymer (1-10%) and a large percentage of water [34]. They provide good encapsulation of cells while still allowing oxygen and nutrient permeation [34]. Also, they can mimic the stiffness of most soft tissues [44]. Higher concentrations of polymer can be used to improve the mechanical properties of the hydrogel, but the resulting increase in stiffness can have negative effects on cell migration [45].

Both naturally-derived and synthetic polymers can be used in hydrogels, but synthetic polymers tend to offer more tailorable and reproducible mechanical properties [41, 46]. Examples of synthetic polymers that have been thoroughly studied as bioinks include

polyethylene glycol (PEG) [20, 47], methacrylated gelatin [48], and pluronic acid-based materials [49]. However, natural polymers tend to better support cell viability and growth [41]. Naturally-derived hydrogels can consist of either animal or plant-based materials. Animal-derived materials typically show greater cell growth and function due to the signaling cues and binding sites that are present in them [41]. Natural polymers that have been used as bioinks include agarose [43], alginate [21, 50-52], cellulose [50, 51, 53], chitosan [5, 54], collagen [55], decellularized extracellular matrix [56], fibrin [21, 57], gelatin [21], hyaluronic acid [22, 27, 53], and silk [58]. This project focused on the use of alginate, cellulose, and gelatin in hydrogel bioinks.

Alginate is a linear heteropolysaccharide consisting of various patterns of D-mannuronic and L-guluronic acid units [59]. It is derived from the cell walls of seaweed or algae [41, 44, 59]. Often times, it is modified with various salts to make it more stable in water [59]. Sodium alginate is a common example of this, and it has found many uses in biomedical applications because of its biocompatibility, ease of use, and low price. For bioprinting, it has shear thinning properties, but it forms a soft gel [41]. This leads to poor shape fidelity and limits the height of bioprinted constructs. To address this, alginate is commonly crosslinked using sodium-calcium ion exchange. Additionally, prefabricated or sacrificial scaffolds can be used to better support the print [60]. Blending with larger molecules like cellulose has also been studied to improve its printability [47, 51]. In terms of physiological properties, alginate has been shown to provide cell viabilities ranging from 90-94% when printing chondrocytes and osteoblasts [60]. This can likely be partly attributed to the ability of alginate to shield and protect cells from shear forces during the printing process. However, alginate does not have cell binding domains, which limits the amount of cellular attachment and proliferation that can occur [41]. In human adipose derived

stem cells, chemical modification using peptides improved cell attachment and integrin expression [52]. Alginate has been shown to be compatible with many different cell types including neural stems cells, skeletal myoblasts, and articular chondrocytes among others [34].

Cellulose is a linear polysaccharide consisting of repeating glucose units connected by β 1-4 glycosidc bonds [61]. It can be obtained from the cell walls of many plants and algae, but mechanical and chemical processing are often required to isolate the cellulose and remove other components, namely hemicellulose and lignin. Alternatively, it can be produces by different organisms including bacteria and tunicates [61]. Properties of sustainability, biocompatibility, and biodegradability have led to significant interest in cellulose in biomedical fields [62]. For bioprinting, nanocellulose has been extensively studied because of its desirable mechanical properties such as high aspect ratio and shear thinning, which make it an intriguing candidate as a viscosity modifier in bioinks. Nanocellulose can occur in the form of cellulose nanofibers (CNFs) or cellulose nanocrystals (CNCs), which require additional processing to remove the amorphous regions and obtain highly crystalline rod-shape particles [61]. This processing can, however, be costly and time intensive, induce batch to batch variation, and result in chemical changes along the cellulose backbone. Additionally, cellulose provides poor cellular attachment because it does not have cell binding domains [51]. To improve its properties when creating bioinks, cellulose is commonly blended with materials like hyaluronic acid [53] or alginate [50, 51]. Nevertheless, cell viability of human nasoseptal chondrocytes has been shown to increase from 73 to 86% over the course of seven days of culture in cellulose-based bioinks [50].

Gelatin is a denatured protein that is commonly derived from the skin of fish, pork, or calves by hydrolyzing collagen using partial acid or alkaline hydrolysis [41, 63]. It is a large molecule consisting of cationic, anionic, and hydrophobic groups [63]. It has been widely used in

biomedical and pharmaceutical industries because of its desirable biocompatibility, biodegradability, and easy chemical modification [63]. These properties have made it an obvious candidate to transition into the field of bioprinting. In terms of mechanical properties, gelatin tends to have poor printability and shape fidelity, and it experiences a sol-gel transition under physiological conditions (37°C and high humidity) leading to a low viscosity [41]. Blending with alginate, hyaluronic acid, fibrin, or silk can improve the stability of gelatin during incubation while also improving its printability [41]. Gelatin's physiological properties of good biocompatibility, biodegradability, and available cell binding domains help to promote cell adherence, differentiation, migration, and proliferation [34, 41]. These are important characteristics in creating bioprinted constructs that not only mimic in vivo structure but also functionality. For example, a gelatin-fibrinogen bioink printed with dermal fibroblasts has facilitated cellular functions like collagen production, cellular infiltration, and biodegradation [57].

### 2.4. Current and Potential Applications for Bioprinting

As the field of bioprinting continues to grow and develop, it offers many possibilities for the future. Arguably the most exciting outlook for the field would be the ability to print any human organ for transplant, which would help solve the growing issue of organ shortage. Unique organs could be printed for an individual based on a scan of the patient's own organ. Using the methods mentioned earlier, various tissue structures have already been bioprinted at the lab scale including skin [64], cartilage [65], blood vessels [66], bone [67], ears [68], and tracheal grafts [69]. Additionally, tissue engineered bladders produced by two-step biofabrication have been successfully transplanted into patients, showing a potential area for the growth of bioprinting [70].

More complex organs like the heart, liver, kidneys, and pancreas still need more research before they can be accurately bioprinted. Fully functional solid organs present many challenges due to their complex heterogeneous architectures that contain multiple functioning cell types. For many of these applications, most of the current hydrogels have been found to be deficient in their mechanical make-ups as they are either too soft to survive interaction with heat induced printing or they lack the flexibility and elasticity needed for the creation of a vascular network.

Development of functional blood vessels will be essential for the construction of artificial organs because they are required for the transportation of nutrients, oxygen, and waste to and from cells in the deeper layers of tissues. Typically, any cell in the human body is only 100 to 200 micrometers away from the nearest blood vessel to allow for the necessary diffusion [71]. In bioprinting or tissue engineering, tissues of more than a few hundred microns cannot be sustained because of a lack of oxygen flow [44]. Bioprinted vascular networks will need to be compatible with that of the patient so that they can be easily engrafted [34]. Additionally, some tissues will require external conditioning such as mechanical pulsing or flow. For example, perfusion bioreactors have been used to simulate blood flow in vessels, which helps to stiffen the vessels and increase their pressure thresholds [72]. Tensile conditioning has been used to improve fiber alignment and increase strength in skeletal muscles [73]. Once many of these challenges have be accomplished, functional bioprinted organs may not be that far away.

A building block on the way to transplantable bioprinted organs is the use of bioprinted tissues for drug testing. This will allow for the industry to continue to develop without yet having to consider all the risks associated with transplanting an organ into a patient. Currently, many drugs are preclinically tested on either two-dimensional cell cultures or animals. Two-dimensional testing methods do not accurately replicate how cells will interact with each other

and with their surrounding extracellular matrix [3], and drug formulations diffuse much more quickly through two-dimensional cultures than in three-dimensional tissues. Also, animal cell proliferation and pathophysiology conditions differ from that of human cells [74].

These shortcomings can lead to poor indicators of how a certain drug will affect human cells. By bioprinting cells into a three-dimensional structure, the efficiency of drug testing could be improved, which would help to lower costs and reduce the time drugs spend in preclinical trials [74]. Various types of small tissue models have already been developed to help in drug development, cancer research, and toxicology screenings [20-27]. Studies like these provide a basis and direction for continued growth of bioprinting not only for drug testing but also for organ tissue engineering in the future.

# 3. MATERIALS AND METHODOLOGY

## 3.1. Materials

### 3.1.1. Cell Culture Materials

Dulbecco's modified eagle media (DMEM), Seradigm fetal bovine serum (FBS), and phosphate buffered saline (PBS) were purchased from VWR (Sanborn, NY, USA). Antibiotic antimycotic solution was obtained from Corning (Manassas, VA, USA). Cell culture media was created by combined 89% DMEM, 10% FBS, and 1% antibiotics. Trypsin EDTA, 0.25% solution, was purchased from HyClone (Logan, UT, USA), and trypan blue, 0.4% solution, was purchased from Lonza (Walkersville, MD, USA). BxPC-3 pancreatic cancer cells were obtained from the American Type Culture Collection (ATCC) (Manassas, VA, USA). Two different cell viability assay kits were tested. Viability/cytotoxicity assay kits for animal live & dead cells were purchased from Biotium (Freemont, CA, USA), and ReadyProbes cell viability imaging kits, blue/green, were purchased from ThermoFisher Scientific (Waltham, MA, USA).

### 3.1.2. Bioink Materials

CNCs were provided by the Forest Products Lab (FPL) (Madison, WI, USA) and CelluForce (CF) (Windsor, QC, CA). Carboxymethyl cellulose (CMC) sodium salt, medium viscosity, was ordered from MP Biomedicals (Solon, OH, USA). Gelatin was purchased from Zint (New Hampton, NY, USA), and alginic acid sodium salt, high viscosity powder was purchased from Alfa Aesar (Ward Hill, MA, USA). A 90 mM calcium chloride ($CaCl_2$) crosslinking solution was created by dissolving $CaCl_2$ from Willpowder (Miami Beach, FL, USA) in deionized water.

## 3.2. Methodology

### 3.2.1. Printer Parameter Optimization

A number of parameters play critical roles in achieving consistent, uniform prints. These include slicing software inputs of print speed, line width, layer height, and fill pattern, which control the conversion of CAD models in the form of STL files into the g-code required to control printer movements. Other parameters include physical variables of the printer such as nozzle diameter, print temperature, and print pressure, which can be adjusted manual during the print. Various combinations of the aforementioned properties were tested to achieve both smooth printability and good cell viability. Figure 5 depicts the Cellink Inkredible + bioprinter (Gothenburg, Sweden) that was used to print the constructs as well as an example of the toolpath used to print a three-dimensional scaffold. The toolpath was created by converting a CAD file from Autodesk Inventor (San Rafael, CA, USA) to g-code using Slic3r software. A commercial bioink, Cellink Start, was used to print the structures and optimize the parameters.

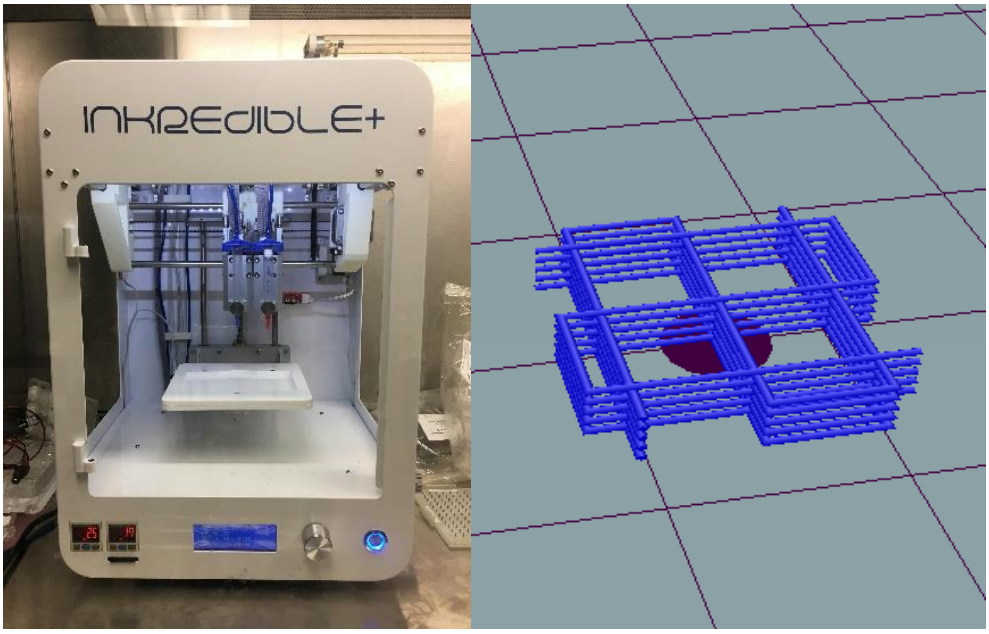


Figure 5. Cellink Inkredible + bioprinter (left) and toolpath used to print a three-dimensional scaffold (right).

### 3.2.2. Optimization of Bioink Formulation

To determine the optimal bioink formulation, various material combinations were tested to evaluate their properties. As mentioned previously, printability, shape fidelity, and biocompatibility are crucial properties of a good bioink. Shear thinning properties are desirable as they allow for a decrease in viscosity and provide uniform flow through the print nozzle when pressure is applied, resulting in good printability. Once the pressure if removed, the viscosity will increase, providing a more stable structure and better shape fidelity. Shear thinning can also improve cell viability by reducing the required printer pressure and thus limiting the shear stresses that cells experience.

Cellulose shows good shear thinning properties while also being inert and therefore nontoxic. Sodium alginate is commonly used in hydrogel bioinks because of its wide availability, biocompatibility, and ease of crosslinking using sodium-calcium ion exchange. However, both cellulose and sodium alginate are plant-based materials that lack cell binding sites to allow for cell attachment. Gelatin is an animal derived material that provides good biocompatibility and provides the cell binding sites that are unavailable in cellulose and sodium alginate.

In an attempt to utilize the advantageous properties of each material, various formulations of cellulose, gelatin, and/or sodium alginate were tested to determine what formulation provided the best printability and shape fidelity. To synthesize the bioinks, the desired concentration of cellulose or gelatin was first added to deionized water and mixed using magnetic stirring for 30 minutes or until a uniform solution was obtained. Then sodium alginate was slowly incorporated, and any aggregates were manually broken up until a uniform gel formed. The bioinks were sterilized at 121°C using the liquid setting of a BioClave 16 autoclave (Benchmark Scientific,

Edison, NJ, USA) before cell culture use. The name and formulation of each bioink tested are displayed in Table 1.

Table 1. Summary of bioink names and formulations.

| Bioink Name | Water (w/v%) | Gelatin (w/v%) | Alginate (w/v%) | Cellulose (w/v%) | Cellulose Provider |
|---|---|---|---|---|---|
| CMC-Al | 94 | 0 | 2 | 4 | MP Biomedicals |
| FPL-CNC-Al | 94 | 0 | 2 | 4 | Forest Product Lab |
| CF-CNC-Al | 94 | 0 | 2 | 4 | CelluForce |
| Gel-Al | 93 | 5 | 2 | 0 | N/A |
| Gel-Al-CNC | 92.5 | 5 | 2 | 0.5 | Forest Products Lab |

#### *3.2.2.1. Rheology Testing*

Rheology testing was performed using a TA Instruments AR-G2 rheometer (New Castle, DE, USA), which can be seen in Figure 6. All tests were performed at room temperature using 25-mm diameter parallel plate attachments and a 300-µm gap. At least three replications were performed for each test, and the average was calculated. To study the viscosity of the samples, steady state flow tests were performed where the shear rate was varied from 0.1 to 500 $s^{-1}$. To determine the linear viscoelastic region (LVR) of the hydrogels, a strain sweep from 0.01 to 100% strain was performed at a frequency of 1 Hz. If the hydrogel did not leave the LVR in this strain range, the range was further increased for that bioink formulation. The end of the LVR was defined as the strain value where the complex modulus of the hydrogel decreased by 10% from the constant plateau value [75]. Lastly, frequency sweeps from 0.01 to 10 Hz were conducted at strain values determined to be in the LVR from the strain sweeps.


Figure 6. TA Instruments AR-G2 rheometer with parallel plate attachments used to perform rheological testing.

Theoretical calculations were used to compare the rheological results to the shearing that occurs in the nozzle during printing. The shear thinning properties of the bioinks were modeled using the power-law model, which is shown in Equation 1.

$$\eta = K\,\dot{\gamma}^{n-1} \tag{1}$$

where η is the apparent viscosity, K is the fluid consistency, $\dot{\gamma}$ is the shear rate, and n is the flow behavior index. Curve fitting was performed on the viscosity versus shear rate curves to calculate the values of K and n for different bioinks. To compare the viscosity of each bioink during printing, the shear rate in the nozzle was calculated. The Rabinowitsch correction was used to account for the non-Newtonian behavior of the bioinks, which is given by Equation 2.

$$\dot{\gamma} = \frac{4Q}{\pi r^3}\left(\frac{3}{4} + \frac{1}{4n}\right) \tag{2}$$

where $\dot{\gamma}$ is the shear rate, Q is the volumetric flow rate, r is the radius of the nozzle, and n is the flow behavior index. The average shear rate at the tip of the nozzle was calculated by numerical

integration of radii from 205 to 500 μm using the measured flow rates of 13.5 and 9.9 μL/s for bioinks CF-CNC-AL and CMC-AL respectively. Lastly, the average viscosity of the bioinks through the tip of the nozzle was calculated from Equation 1 using the calculated shear rates.

#### *3.2.2.2. Confocal Microscopy*

Scaffolds of bioink CF-CNC-Al were prepared into molds and soaked in EpoDye from Struers Inc. (Cat. # 40300002, Cleveland, OH, USA). The prepared molds were visualized with a Zeiss LSM 700 laser scanning confocal microscope (Thornwood, NY, USA) using Plan-Apochromat 40x/1.3NA oil immersion lens and 20x/0.8NA objective lens where the 488/520 nm green channel was assigned for the dye. For 3D visualization, Z-stack images were taken up to 80 μm deep into the mold structure. Computation of the Z-stack images was performed in Imaris (9.0.1) (Bitplane, South Windsor, CT, USA) software to obtain rendered reconstructions of the pores. The National Institutes of Health (NIH) ImageJ software was used to analyze the porosity and average pore diameter of the images.

### 3.2.3. Design of Bioreactor

To simulate vasculature in the body, a bioreactor was designed to provide media circulation. This was done to increase the rate of diffusion through the hydrogel scaffolds and to improve drug dispersion throughout the wells. The bioreactor was 3D printed to allow for quick optimization and alterations while also providing an economical option compared to commercial bioreactors. Initially, a perfusion bioreactor was designed as it closely mimics the flow of blood around the tumor microenvironment; however, it was difficult to scale up the perfusion bioreactor design. Therefore, a spinning bioreactor was designed to circulate the media and increase the diffusion rate. Figure 7 depicts the structure of the spinning bioreactor, which was adapted from a previous study [76]. The mixers, plate cover, and top motor support were

manufactured using a Formlabs Form 2 printer (Somerville, MA, USA) while the gears, bearings, fasteners, and electrical components were purchased from commercial vendors.

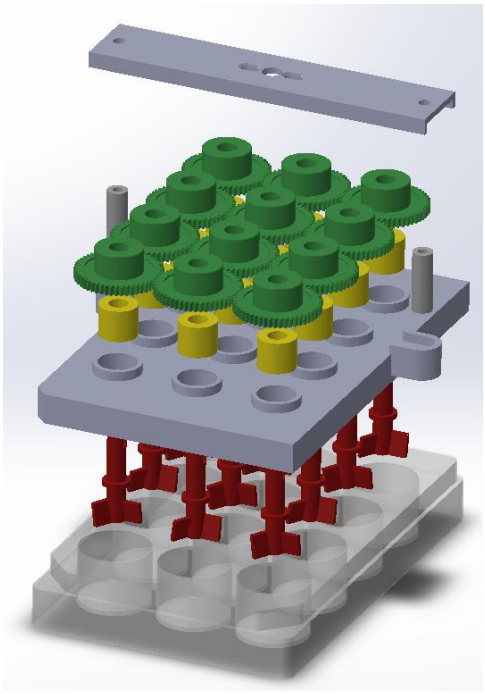

Figure 7. Exploded view of the spinning bioreactor design where the 3D printed cover and mixers fit over and into a standard 12 well plate.

### 3.2.4. Analysis of Cell Viability in Bioprinted Scaffolds

To prepare the cells and bioink for printing, cell culture media containing BxPC-3 cells was mixed with bioink at a ratio of 1:10. It was determined that a final concentration of $1 \times 10^6$ viable cells/mL was a reasonable cell density for this application. Scaffolds were then printed directly into a 12 well plate with each scaffold requiring about 0.5 mL of bioink resulting in a final cell density of approximately $5 \times 10^5$ viable cells/scaffold. The scaffolds were then crosslinked using a 90 mM $CaCl_2$ solution for 5 minutes. Following crosslinking, the scaffolds were washed twice with PBS and then incubated in cell culture media. The media on the scaffolds was refreshed every two days.

To determine cell viability in the scaffolds, a procedure outlined in a previous protocol was followed [77]. First, a 4 µM calcein AM/8 µM EthD-III solution was prepared by combining 2 µL of 4 mM calcein AM, 8 µL of 2 mM EthD-III, and 2 mL PBS. The scaffolds were washed and incubated in DMEM without FBS for 30 minutes. Then the DMEM was removed, and the scaffolds were fully covered in the staining solution (2 mL per scaffold) and incubated for 1 hour. Next, the staining solution was removed, and the scaffolds were washed twice and incubated again in DMEM without FBS for 30 minutes. Lastly, the scaffolds were transferred to a microscope slide and imaged by fluorescence microscopy (Leica DMi8, Wetzlar, Germany) using the FITC, Texas Red, and DAPI filters.

Cell viability was calculated from the resulting images using NIH ImageJ software. First, the images were opened and converted to greyscale. Then a threshold was set so that only the cells were shown, and the background noise was removed. Next, the required size of the cells was input, and the cells were automatically counted by the software. Images at three different locations were analyzed for each scaffold. Figure 8 on the next page outlines the process of counting cells using ImageJ. It starts with the composite fluorescence microscopy image, then moves to the individually filtered images, and finally shows the final cell counts both in their images and in the summary box.

From the ImageJ cell counts, the percentage cell viability was calculated by using Equation 3 below. Two scaffolds were tested for each time point, and the average was calculated.

$$Cell\ Viability\ (\%) = \frac{Live\ Cells}{Live\ Cells + Dead\ Cells} * 100 \quad (3)$$

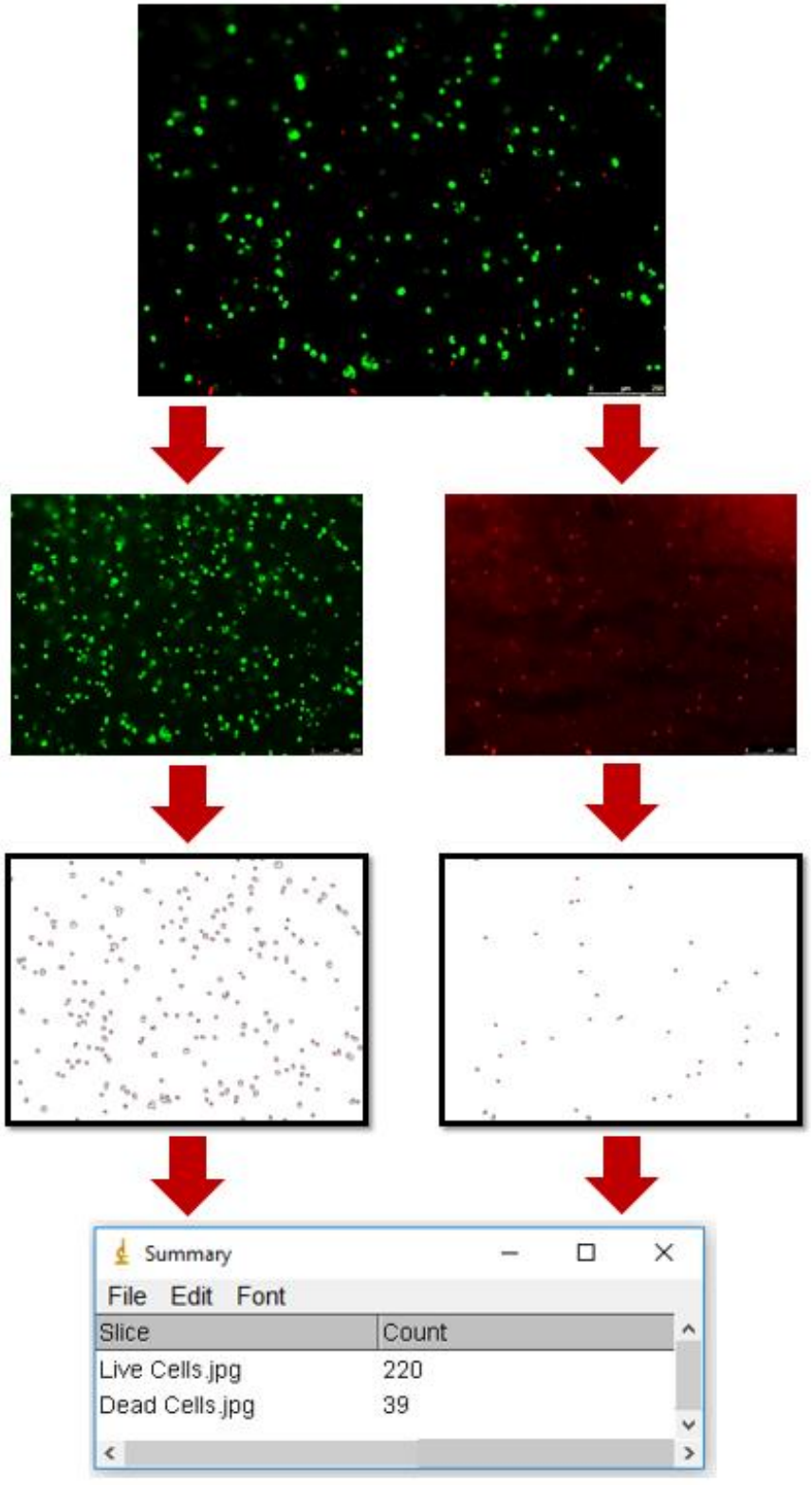


Figure 8. Process of counting live (green) and dead (red) cells from fluorescence microscopy images using NIH ImageJ software.

# 4. RESULTS AND DISCUSSION

## 4.1. Printer Parameter Optimization

Various geometries and architectures were printed to evaluate the effects of different printing settings on printability and shape fidelity. It was determined that both g-code control parameters (print speed, line width, layer height, fill pattern) and physical printer parameters (nozzle diameter, print temperature, print pressure) play important roles in high resolution printing. Table 2 displays the final printer settings.

Table 2. Summary of final printer parameters.

| **Slic3r Parameters** | |
|---|---|
| Print Speed | 5 mm/s |
| Line Width | 0.7 mm |
| Layer Height | 0.5 mm |
| Fill Pattern | Rectilinear |
| **Printer Parameters** | |
| Nozzle Diameter | 22 G (410 µm) |
| Print Temperature | Room Temperature |
| Print Pressure | 25 kPa |

Print pressure has a significant impact on cell viability during the printing process as higher pressures result in higher shear stresses on the cells [42]. Because of this, the largest standard nozzle size of 22 G was chosen. Additionally, it was found that smaller nozzles were more prone to clogging. From there, the print pressure was manipulated to determine what pressure was required to achieve uniform extrusion. It was found that a pressure of 25 kPa was adequate to achieve smooth flow out of the nozzle, and similar or higher pressures have been shown to produce high cell viabilities in other studies [50, 51]. Next, the print speed was determined as it is affected by both nozzle diameter and print pressure. Too slow of a print speed

can result in over-extrusion of material and poor print resolution, while too fast of a print speed can result in thinning and potentially breakage of the gel filament [78].

Line width and layer height mostly depend on the nozzle diameter. However, bioink rheological properties also play a role as some materials spread on the print bed due to gravity more than others. This spreading results in a lower layer height compared to the line width. For the nozzle size and material tested here (Cellink Start bioink), a layer height of 0.5 mm and a line width of 0.7 mm were selected. When lower layer heights or line widths were tested, over-extrusion and overlapping of material occurred. On the contrary, larger layer heights or line widths resulted in gaps between the material, and the gel filament had a greater tendency to break away from the printed structure, which frequently resulted in curling at the nozzle tip.

Lastly, different fill patterns including rectilinear and concentric were evaluated to see what would provide the best print resolution and shape fidelity. It was determined that rectilinear was more effective for print geometries with many straight lines or sharp corners while concentric was a better choice for geometries with more curved or round features. Since the scaffolds used for this application were rectangular with mostly straight lines, the rectilinear fill pattern was chosen. These parameters were then verified by printing a variety of geometries including a cube, a hollow cylinder, and a pancreas model, which can be seen in Figure 9.


Figure 9. Different print geometries that were used to verify the printer parameters including a) a cube, b) a hollow cylinder, and c) a pancreas model.

## 4.2. Optimization of Bioink Formulation

### 4.2.1. Printability

Scaffolds of each bioink were printed to evaluate the printability and shape fidelity of each. Bioink CMC-Al showed poor print resolution as any scaffold printed with more than one layer would flow together once deposited on the print bed. Bioink FPL-CNC-Al, which contained CNCs from the FPL instead of CMC, provided better print quality as multiple layers could be printed while still maintaining pores for nutrient and waste diffusion. Additionally, bioink FPL-CNC-Al required a lower pressure of 25 kPa to print compared to 50 kPa for bioink CMC-Al. This can likely be attributed to the better shear thinning properties of CNCs compared to CMC, which are discussed further in section 4.3.1 Rheology Testing. Figure 10 shows a comparison of the scaffolds printed using each bioink.

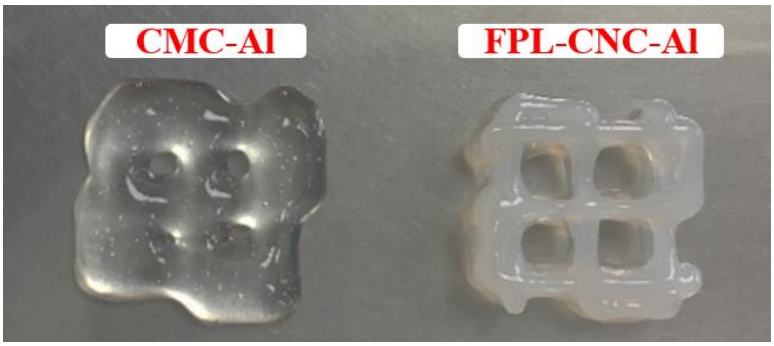


Figure 10. Scaffolds printed with bioinks CMC-Al (left) and FPL-CNC-Al (right).

To compare different CNCs, bioinks CF-CNC-Al and FPL-CNC-Al were tested to determine the effects of the CNC processing technique on bioink properties. In terms of printability, both bioinks showed very similar properties and printed at 25 kPa. Figure 11 shows a comparison of scaffolds printed with the different CNC bioinks.

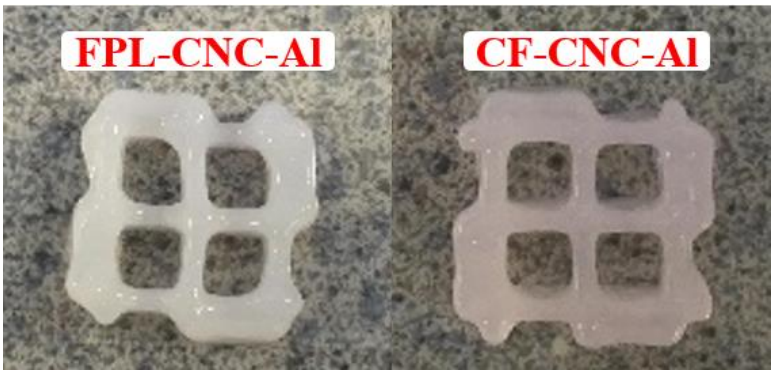


Figure 11. Scaffolds printed with bioinks FPL-CNC-Al (left) and CF-CNC-Al (right).

When testing the printability of gelatin as the major bioink component as opposed to cellulose, bioink Gel-Al showed a stable structure with minimal spreading on the print bed. However, the bioink did not flow smoothly out of the nozzle, which resulted in a more jagged print geometry, and a pressure of 65 kPa was required. In an attempt to improve its printability, CNCs were added to create bioink Gel-Al-CNC. This resulted in a more uniform, smooth print and reduced the print pressure slightly to 60 kPa. Figure 12 compares the scaffolds printed using bioinks Gel-Al and Gel-Al-CNC.

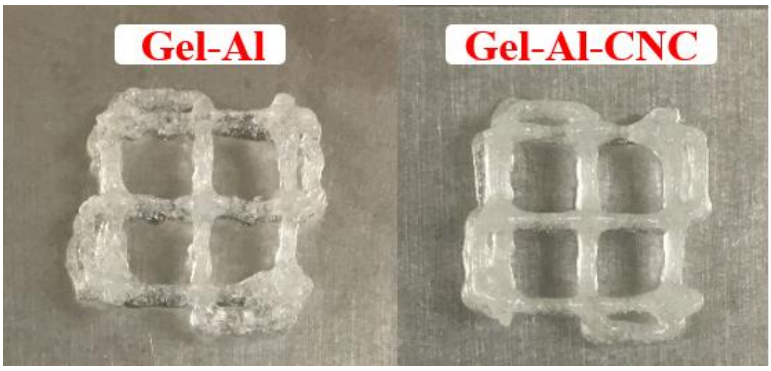


Figure 12. Scaffolds printed with bioinks Gel-Al (left) and Gel-Al-CNC (right).

Based off printability, bioink CMC-Al was eliminated because of its tendency to flow once deposited on the printed bed. The remaining four bioinks underwent further testing to determine which would provide the best option for three-dimensional cell culture drug testing applications.

### 4.2.2. Cell Visibility

It is important that cells are clearly visible through the three-dimensional structure so that accurate cell viabilities can be determined. Cell visibility in bioinks FPL-CNC-Al, CF-CNC-Al, Gel-Al, and Gel-Al-CNC were compared using two different cell viability kits including a blue-green kit from ReadyProbes (ThermoFisher Scientific, Waltham, MA, USA) and a green-red kit from Biotium (Freemont, CA, USA). In the ReadyProbes kit, the nuclei of the living cells are dyed blue while the nuclei of the dead cells display a blue-green color. In the Biotium kit, the cytoplasms of the live cells are dyed green, and the nuclei of the dead cells are dyed red.

Bioink Gel-Al-CNC had a translucent nature, which was desirable for imaging by fluorescence microscopy. Figure 13 shows the translucent nature of the bioink as well as a fluorescence microscopy image after using the ReadyProbes kit.

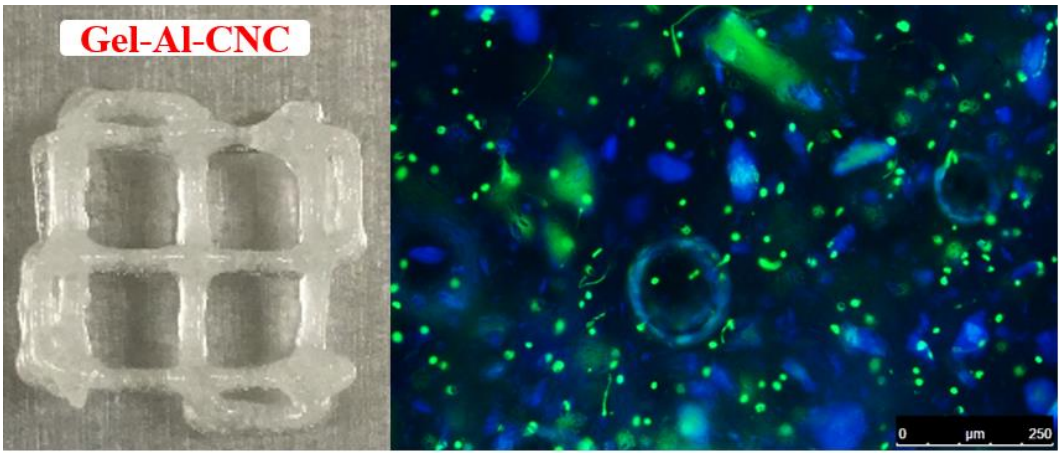


Figure 13. Scaffold printed with bioink Gel-Al-CNC (left) and resulting microscopy image after staining with ReadyProbes kit where excess background noise from the fluorescing cellulose can be seen (right).

When staining cells in bioink Gel-Al-CNC with the ReadyProbes kit, the dead cells were clearly visible, but the live cells were not. It was found that cellulose has an excitation wavelength of 320 nm [79]. This is very close to the excitation wavelength of the blue dye, which is 360 nm, and the similarity in excitation frequency likely lead to unwanted fluorescence

of the cellulose, resulting in excess background noise and unclear images. Therefore, it was determined that the ReadyProbes kit was unsuitable for use with any bioink containing cellulose.

Bioink Gel-Al also had a translucent nature and was tested using the ReadyProbes kit. After dying the cells in this bioink, both the live and dead cells could be visualized. The resulting images contained minimal background noise and allowed for convenient evaluation of cell viability in the scaffolds. Figure 14 shows the translucent nature of the bioink and a fluorescence microscopy image where both the live and dead cells are clearly visible.

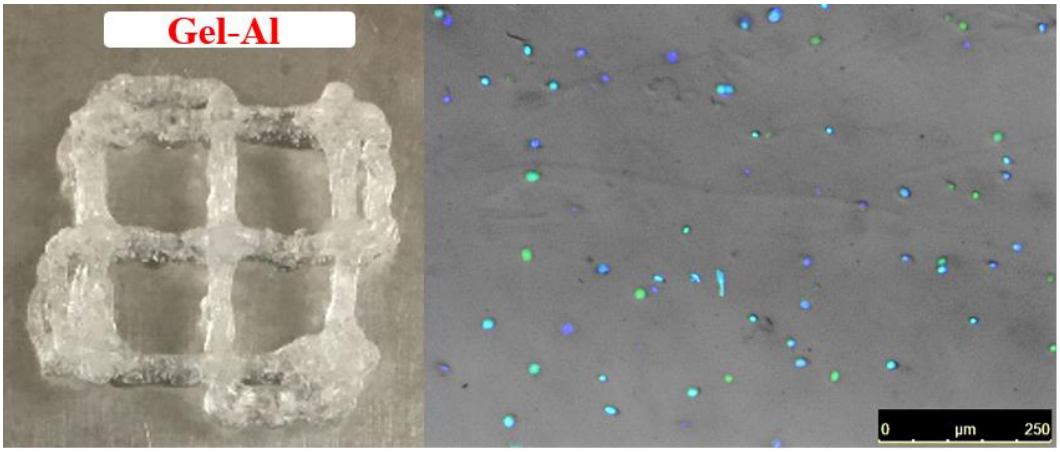


Figure 14. Scaffold printed with bioink Gel-Al (left) and resulting microscopy image after staining with the ReadyProbes kit (right).

When scaffolds of bioink Gel-CNC-Al or Gel-Al were cultured in an incubator for multiple days however, the gelatin dissolved out of the scaffolds, which resulted in an unstable structure. Additionally, these bioinks had frequent contamination issues as autoclave sterilization degraded the gelatin, and ultraviolet sterilization was unsuccessful. Because of these issues, both bioink Gel-Al and bioink Gel-Al-CNC were eliminated from consideration for future drug testing applications.

Both bioink FPL-CNC-Al and bioink CF-CNC-Al had opaque natures making it more difficult to visualize cells through them. To address this, the scaffolds were kept to a low thickness to let as much light as possible pass through them. Figure 15 and Figure 16 show the

opaque nature of bioinks FPL-CNC-Al and CF-CNC-Al respectively as well as their resulting fluorescence microscopy images using the Biotium kit. When staining cells in either of these bioinks with the Biotium kit, the live cells were clearly visible, but the dead cells showed some background noise.

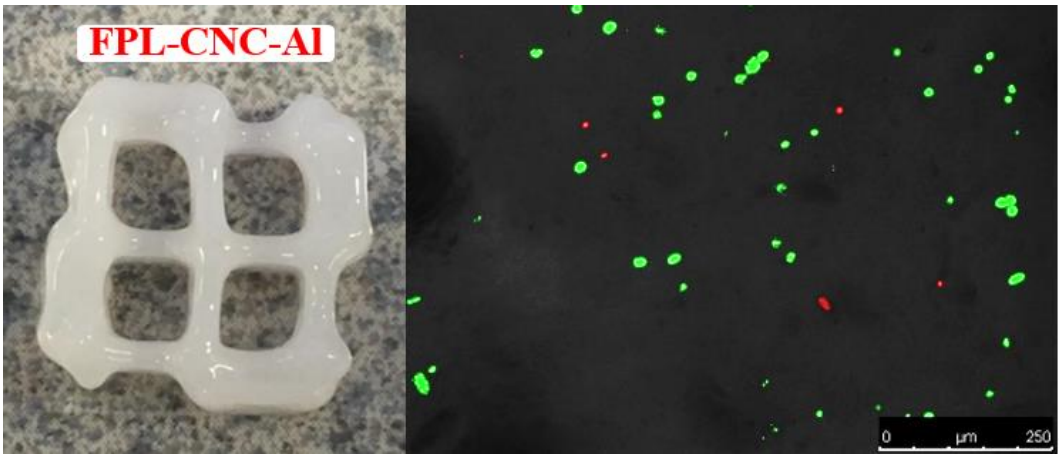


Figure 15. Scaffold printed with bioink FPL-CNC-Al (left) and resulting microscopy image after staining with the Biotium kit (right).

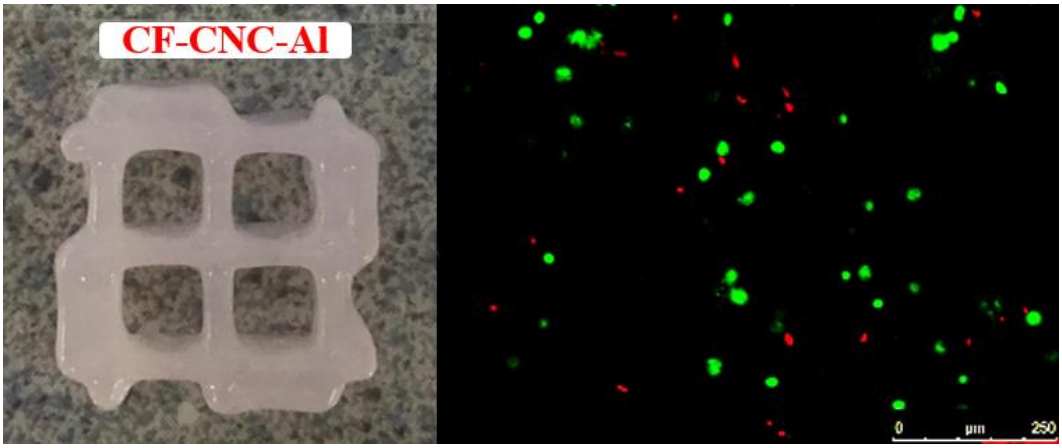


Figure 16. Scaffold printed with bioink CF-CNC-Al (left) and resulting microscopy image after staining with the Biotium kit (right).

The ReadyProbes kit was not tested with these bioinks because of the cellulose fluorescence issues. Based off this testing, bioinks FPL-CNC-Al and CF-CNC-Al were chosen for future testing as they allowed for the best printability, better stability during incubation, fewer contamination issues, and relatively good cell visibility.

### 4.2.3. Cell Viability

Bioinks FPL-CNC-Al and CF-CNC-Al were tested to determine which better supported cell viability and proliferation of BxPC-3 cells. Figure 17 shows a comparison of the resulting cell viabilities for each bioink, and Figure 18 shows the corresponding fluorescence microscopy images. Cell viability after printing in bioinks FPL-CNC-Al and CF-CNC-Al were 74% and 79% respectively. The initial decrease in cell viability after the printing process can be attributed to the handling and shear stresses that the cells experience during the preparation and printing processes. Additionally, the crosslinking process can have negative effects on cell viability because the cells are exposed to high calcium concentrations [80]. Therefore, care should be taken to minimize the crosslinking time and concentration. When culturing the scaffolds for multiple days, bioink FPL-CNC-Al showed a rapid decreased in cell viability compared to bioink CF-CNC-Al. After three days of culture, viable cells were sparse throughout the matrix of bioink FPL-CNC-AL, whereas in bioink CF-CNC-Al, the distribution and number of viable cells were similar to after printing.

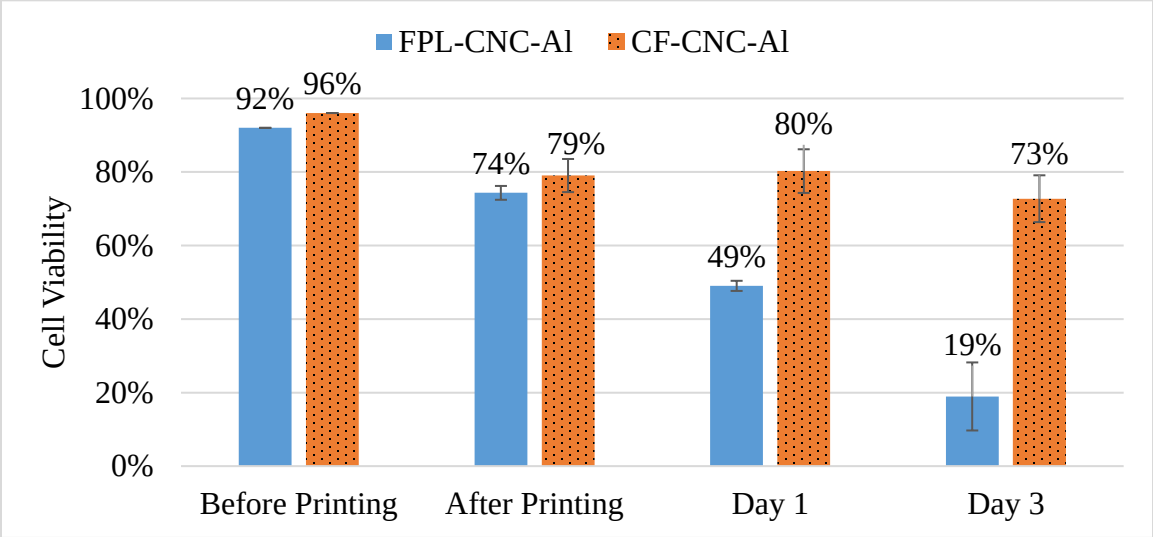


Figure 17. Comparison of cell viability of BxPC-3 cells in bioinks FPL-CNC-Al and CF-CNC-Al.

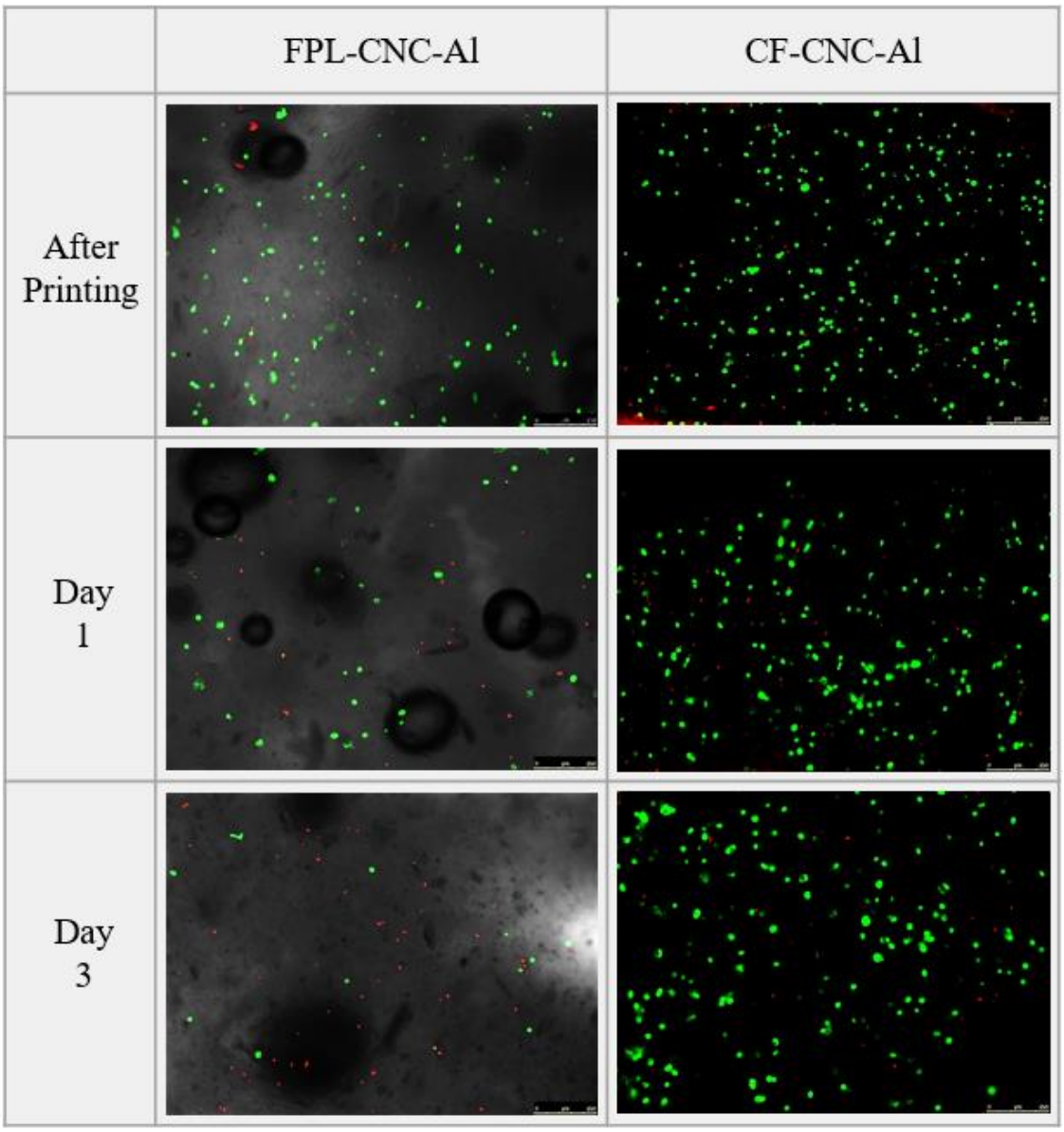


Figure 18. Fluorescence microscopy images of BxPC-3 cells in bioinks FPL-CNC-Al and CF-CNC-Al.

Since both bioinks contained both CNCs and alginate, it was hypothesized that the differences in cell viability could be attributed to the production method used to manufacture the CNCs. Both the FPL and CF manufacture their CNCs using sulfuric acid hydrolysis [81], so the pH of 4% CNC solutions from each manufacturer were measured to determine how well the acid used in the production process had been neutralized. The pH of the FPL CNC solution was 5.62 whereas the pH for the CF CNC solution was 7.32. Therefore, it can be concluded that the poor

cell viability in bioink FPL-CNC-Al can be attributed to the acidity of the CNCs. Other studies have verified that changes in pH can affect cell viability as primary keratinocyte and fibroblast cultures showed complete cell death after one day in culture conditions at pH 5.5 [82]. Based off these results, bioink CF-CNC-Al was chosen for future testing to better evaluate its properties and to test it in conjunction with the spinning bioreactor.

### 4.3. Evaluation of Bioink

Based off the characterization of the bioinks described earlier, Table 3 below shows a comparison of all the bioinks tested and why bioink FPL-CNC-Al was chosen for further evaluation. Each of the bioinks was rated from 1-4 for each property where 1 is poor, 2 is average, 3 is good, and 4 is very good.

Table 3. Comparison of bioink properties.

| Bioink Name | Printability | Cell Visibility | Incubator Stability | Cell Viability |
|---|---|---|---|---|
| CMC-Al | 1 | - | - | - |
| FPL-CNC-Al | 4 | 3 | 3 | 1 |
| CF-CNC-Al | 4 | 3 | 3 | 3 |
| Gel-Al | 2 | 4 | 1 | - |
| Gel-Al-CNC | 4 | 1 | 1 | - |

#### 4.3.1. Rheology Testing

Rheology testing was performed to analyze the response of each bioink constituent to shear forces, which are also experienced during extrusion through the print nozzle. The viscosities of bioink CF-CNC-Al and its individual components were analyzed by steady state flow testing. Additionally, it was compared to bioink CMC-Al and its components to help better understand the difference in printability between bioinks CF-CNC-Al and CMC-Al.

In Figure 19, it can be seen that all of the components and bioinks showed shear thinning behavior, which is represented by a decrease in viscosity over a large range of shear rates with no

apparent plateaus. This is caused by the alignment of polymer chains that occurs when a shear force is applied. Compared to the CMC solution, the CNC solution showed better shear thinning properties as its initial viscosity was slightly higher, and it showed a steeper decrease in viscosity as the shear rate increased. It should be noted as well that the 2% alginate solution showed a higher viscosity than the 4% CNC solution, indicating that alginate had a more substantial effect on the bioink's overall viscosity than the CNCs did.

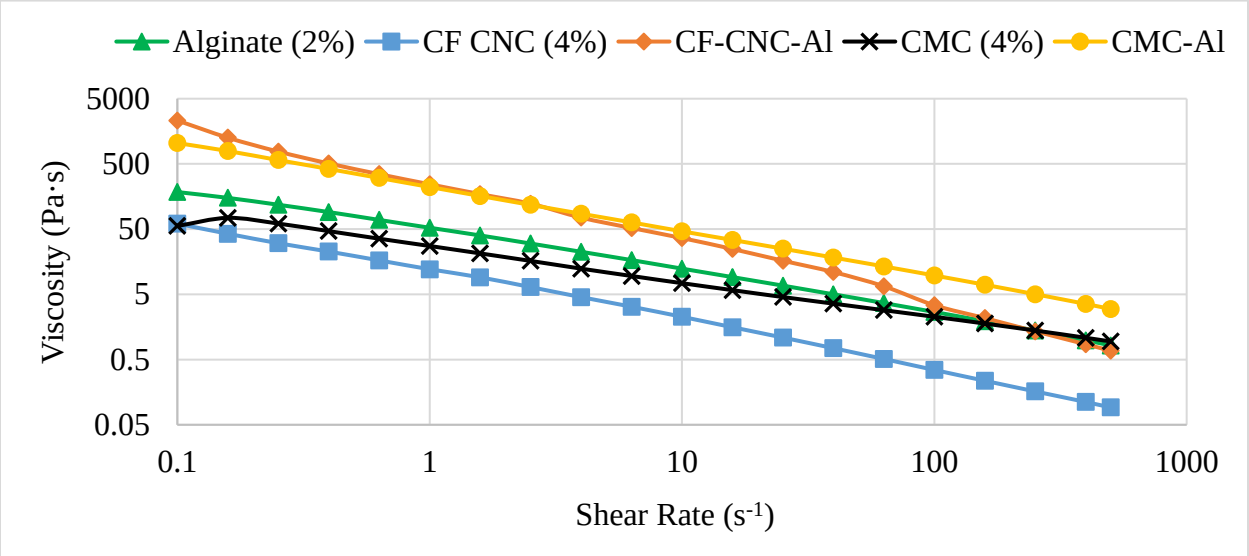


Figure 19. Viscosities of various solutions and bioinks during steady state flow testing.

When comparing bioinks CF-CNC-Al and CMC-Al, the differences in shear thinning can help to explain why bioink CF-CNC-Al showed better printability and can be printed at a lower pressure. Bioinks CF-CNC-Al and CMC-Al showed viscosities of 2314 and 1046 Pa·s respectively at a shear rate of 0.1 $s^{-1}$. At low shear rates like this, a higher viscosity is more desirable so that printed constructs will remain stable and resist spreading on the print bed. Conversely, at higher shear rates such as when the bioinks are being forced through the print nozzle, lower viscosities are more desirable because they allow for smoother flow at lower pressures. From the theoretical calculations, it was determined that bioink CF-CNC-Al has a lower viscosity when it is extruded through the nozzle. Table 4 displays the results of the

theoretical calculations for shearing through the print nozzle. The combination of higher viscosity at rest and lower viscosity at the printing shear rate indicate that bioink CF-CNC-Al is better suited for extrusion bioprinting.

Table 4. Analysis of shear rate and viscosity in the nozzle during printing.

| Bioink | Flow Behavior Index n | Fluid Consistency K | Nozzle Shear Rate ($s^{-1}$) | Viscosity (Pa·s) |
|---|---|---|---|---|
| CF-CNC-Al | 0.078 | 257 | 2350 | 0.20 |
| CMC-Al | 0.315 | 222 | 675 | 2.57 |

Strain sweeps were performed to determine the LVR for each solution, and the results are displayed in Figure 20. The CNC solution showed a sharp decrease in complex modulus as it exited the LVR, which indicates a breakage of the gel into larger pieces, whereas the CMC solution showed a more gradual decrease in complex modulus once it exited the LVR, which indicates a more gradual, homogeneous breakdown of the gel structure. Similar trends are visible for bioinks CF-CNC-Al and CMC-Al respectively.

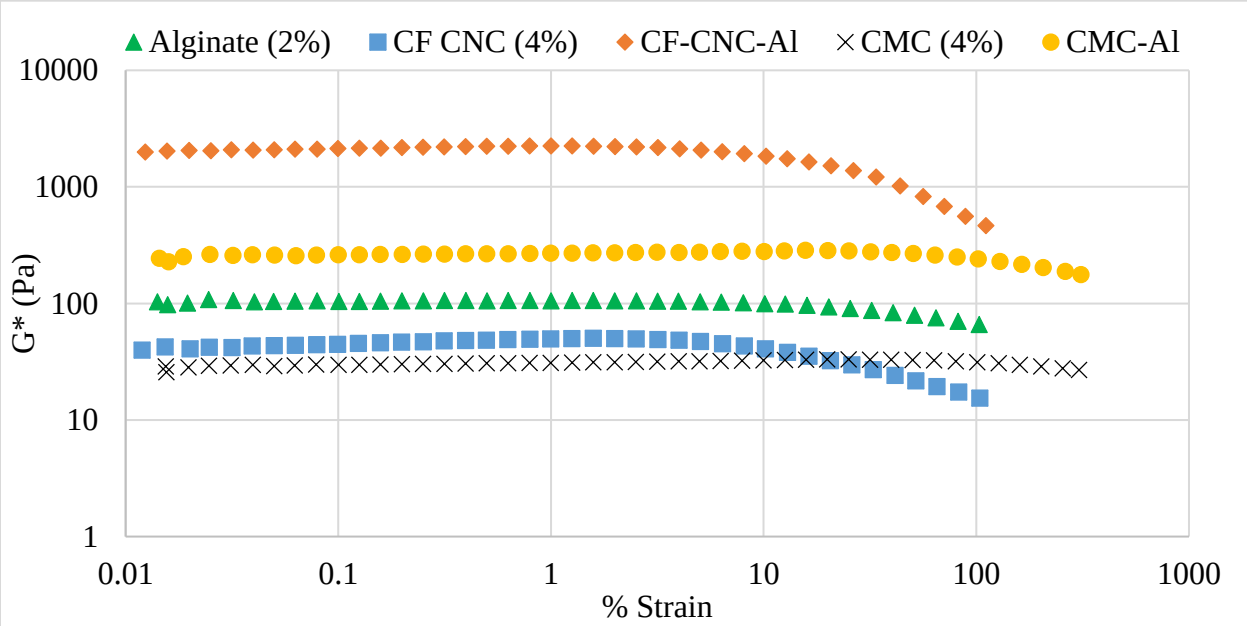


Figure 20. Complex modulus of various solutions and bioinks during strain sweep testing.

Table 5 shows the end of the LVR and the overall strain range that was tested for each solution and bioink. The alginate solution, CF CNC solution, and bioink CF-CNC-Al showed similar LVRs while the CMC solution and bioink CMC-Al were stable at much higher strain values. Based off the strain sweeps, 1% strain was chosen for the frequency sweeps as it fell clearly in the plateau region of the strain sweep for each solution.

Table 5. Strain sweep results for various solutions and bioink formulations.

| Solution | Alginate (2%) | CF CNCs (4%) | CF-CNC-Al | CMC (4%) | CMC-Al |
|---|---|---|---|---|---|
| Strain Range Tested | 0.01 - 100% | 0.01 - 100% | 0.01 - 100% | 0.01 - 300% | 0.01 - 300% |
| End of LVR | 16.01% | 7.52% | 7.52% | 236.33% | 75.46% |

Frequency sweeps for each of the solutions at a constant strain of 1% are displayed in Figure 21. For each case, the storage and loss moduli of each solution increased over the duration of the test. Bioink CF-CNC-Al showed the highest storage modulus throughout the frequency sweep, which is indicative of its higher stiffness or gel strength.

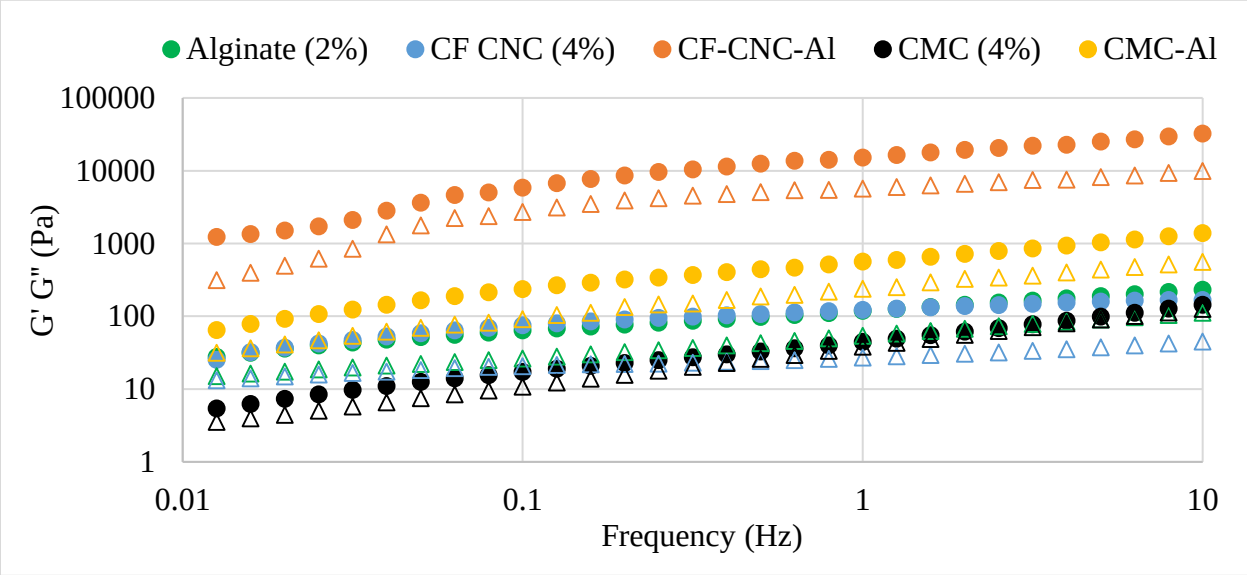


Figure 21. Storage modulus (closed circles) and loss modulus (open triangles) of various solutions and bioinks during frequency sweep testing.

The storage modulus of each solution was greater than the loss modulus over the range of frequencies tested. This indicated that the materials show a more elastic than viscous behavior, and it is also represented by tan delta values of less than one as seen in Figure 22. However, for the CMC solution, the tan delta value was closer to one indicating that the material showed nearly equal elastic and viscous behavior and that it showed more viscous behavior when compared to the other solutions.

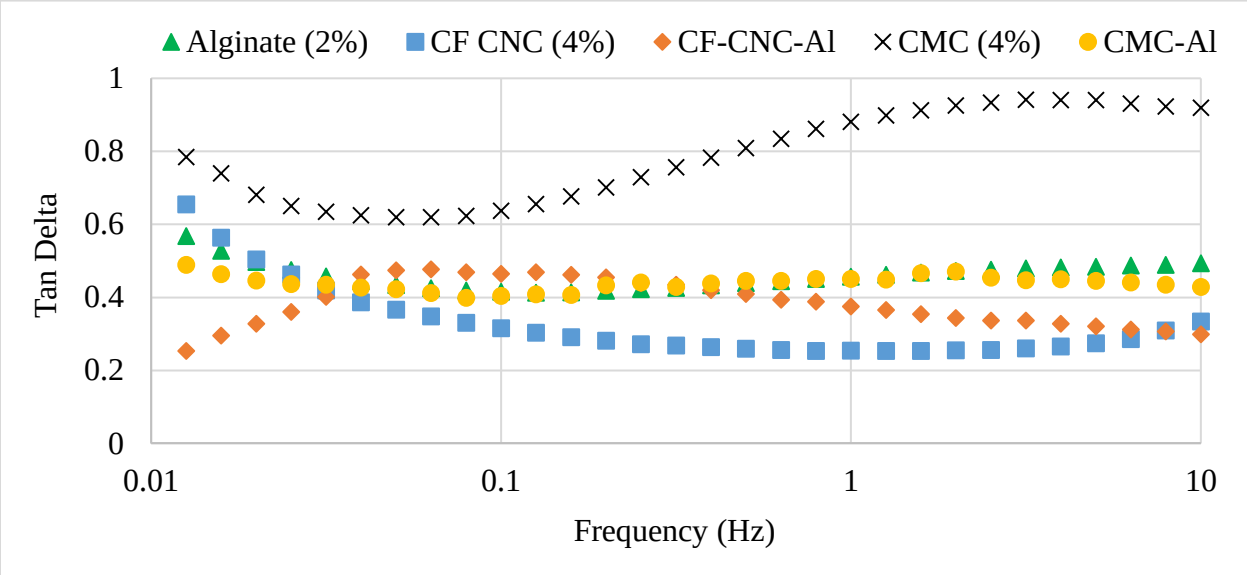


Figure 22. Tan delta values for various solutions and bioinks during frequency sweep testing.

### 4.3.2. Confocal Microscopy

To analyze the porous structure of bioink CF-CNC-Al in its hydrated state, confocal microscopy was performed. Figure 23 and Figure 24 show the resulting microscopy images of the bioink at 40x magnification. The pores in the hydrogel were stained green by the dye while the solid material remained black. The cylindrical and oval pores appear to have uniform distribution throughout the hydrogel; however, the shape of the pores may be altered by the vertical reconstruction that occurs during image processing of the Z-stack images. When analyzing the well stained areas, the hydrogel was found to have an average pore diameter of

12.00 ± 4.48 µm and a porosity of 20.81 ± 2.73%. These pores provide space for nutrients and waste to move in and out of the deeper parts of the scaffold while also providing space for cells to grow and proliferate.

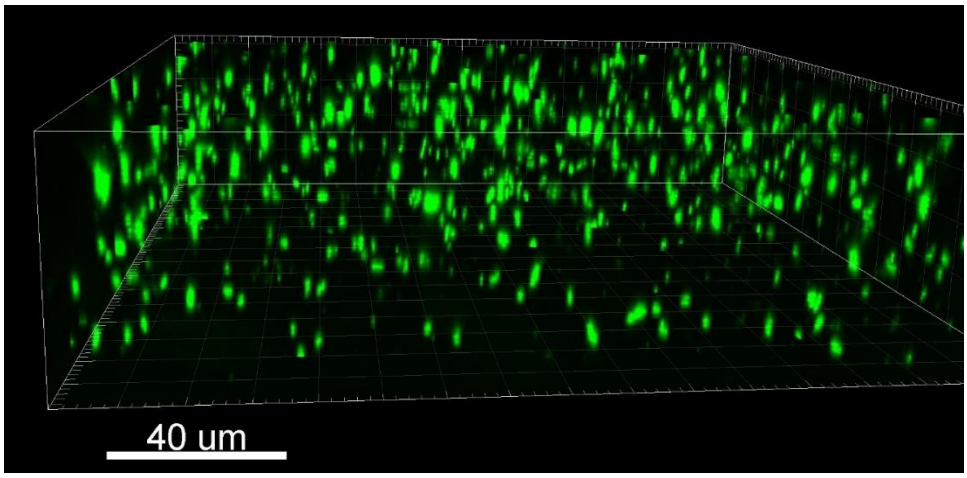


Figure 23. Confocal microscopy image of bioink CF-CNC-AL at 40x magnification showing a lateral view of the pores.

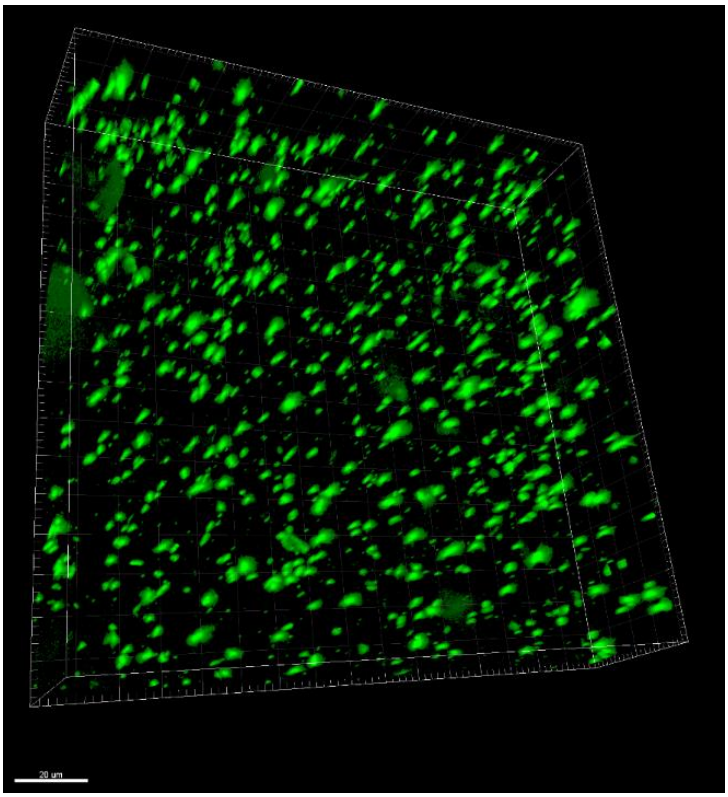

Figure 24. Confocal microscopy image of bioink CF-CNC-AL at 40x magnification showing a top view of the pores. Scale bar is 20 µm.

### 4.4. Design of Spinning Bioreactor

The bioreactor was manufactured to fit over a standard 12 well plate, and the mixers were altered to create room for the scaffolds at the bottoms of the wells. Additionally, drug injection ports were created through the mixers to allow drug formulations to be injected into the individual wells using a micropipette. A speed controller was also added to allow for optimization of the media circulation rate. Figure 25 shows the spinning bioreactor over a 12 well plate with the speed controller, and sample scaffolds printed into the 12 well plate.

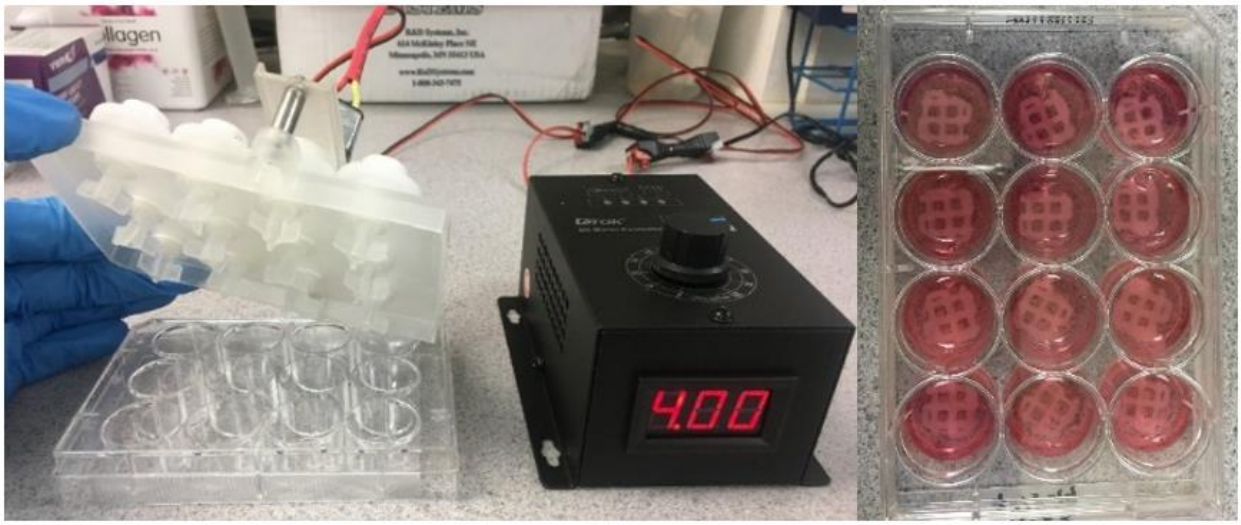


Figure 25. Assembled spinning bioreactor and speed controller (left) and sample scaffolds in a 12 well plate (right).

For each bioreactor, a singular motor distributes power to a gear system that controls the speed of the mixers that fit into each individual well. Figure 26 displays the circuit diagram for the spinning bioreactor system. Two spinning bioreactors were wired in parallel so that they could be controlled by a single speed controller. The speed controller was kept outside of the incubator to allow changes in speed without disrupting the contents of the incubator.

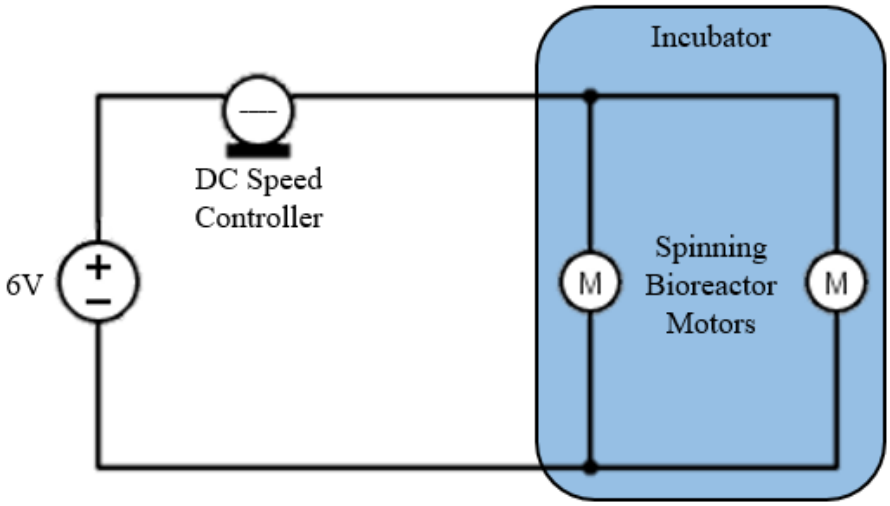


Figure 26. Spinning bioreactor circuit diagram.

To calibrate the spinning bioreactor, voltage readouts from the DC speed controller were plotted against the rotational speed of the mixers, which can be seen in Figure 27. It was determined that the relationship between voltage and speed was linear. The allowable voltage range was from 2.5 to 5.12 volts. Below 2.5 volts, the speed controller does not receive enough power to illuminate the display, and 5.12 volts was the maximum voltage that could be supplied by the AC to DC adapter power supply.

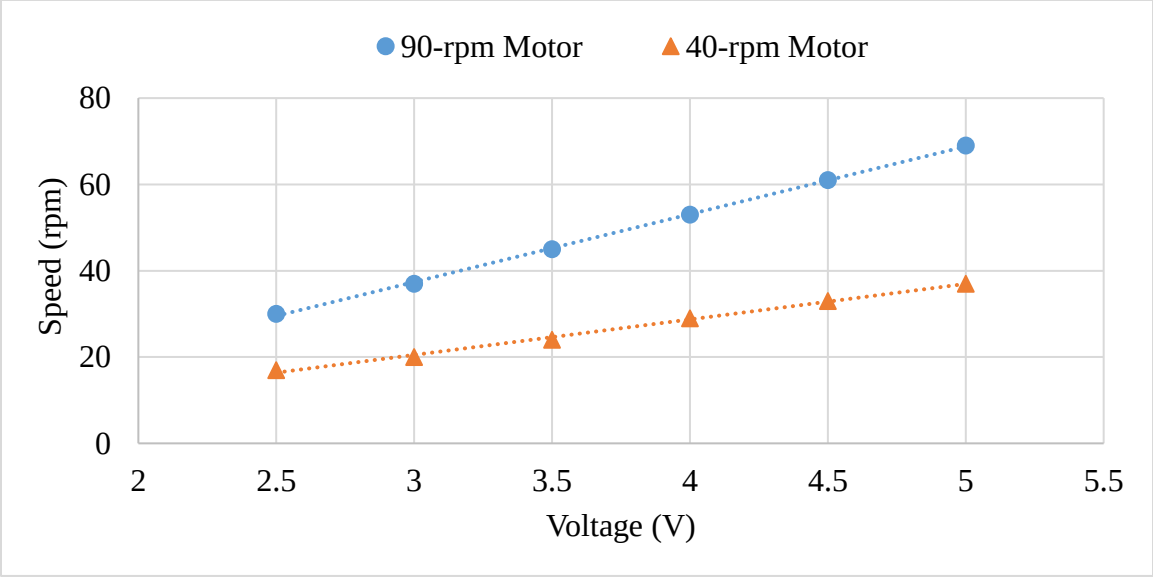


Figure 27. Calibration curves for the spinning bioreactor with different motors.

The calibration curves were used to determine the required voltage readouts to test various bioreactor speeds. For the 40-rpm and 90-rpm motors, the calibration equations were determined to be Equation 4 and Equation 5 respectively.

$$rpm_{40} = 8.23\,V - 4.19 \quad (4)$$

$$rpm_{90} = 15.71\,V - 9.76 \quad (5)$$

where rpm is the rotational speed in revolutions per minute and V is the voltage readout from the speed controller in volts.

### 4.5. Evaluation of Cell Viability Using the Spinning Bioreactor

The spinning bioreactor was tested to determine its effects on cell viability in bioink CF-CNC-Al. Figure 28 shows a comparison of the resulting cell viabilities with and without use of the spinning bioreactor. Initial cell viability was 79% after printing, and it remained fairly stable for the first two days of culture whether or not the bioreactor was used. After day three however, the scaffolds that were cultured with the spinning bioreactor showed a decrease in cell viability. It was observed that a few of the scaffolds were being rotated by the mixers of the bioreactor. Therefore, this decrease in cell viability could likely be attributed to mixers shearing the scaffolds and disturbing the cells in them. To address this, the clearance between the mixers and scaffolds was increased. Additionally, slower mixing speeds of 10 and 20 rpm were tested to try to minimize disturbances on the scaffolds. However, when trying to test these slower bioreactor speeds, initial cell viability after printing was very poor, which was likely caused by significant cell death during the printing process. Since the initial cell viability was nowhere near the 79% that was achieved in previous testing, these results were excluded because they did not make for an adequate comparison against the testing at 50 rpm.

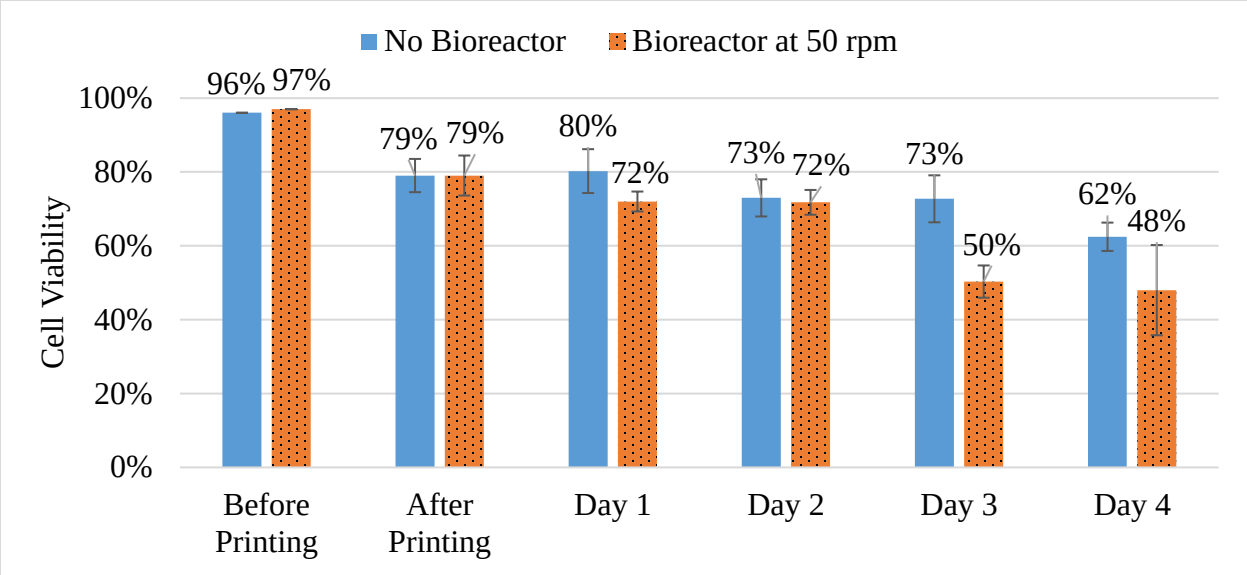


Figure 28. Comparison of cell viability of BxPC-3 cells in bioink CF-CNC-Al with and without use of the spinning bioreactor.

Figure 29 shows the fluorescence microscopy images with and without the spinning bioreactor. When looking at the images without the use of the spinning bioreactor, an increase in size of the green dots, which were assumed to be living cells, can be seen. It is possible that this is due to the formation of small cellular spheroids. Comparing the images from after printing to day four, the average diameter of the green dots increased from 21.18 ± 7.06 to 33.40 ± 10.67 µm. If small spheroids are forming, a different assay should be developed to better analyze cell viability as the current one assumes that each green dot is an individual cell. A possible alternative to this would be an MTT assay, which measures cellular metabolic activity and has been shown to work in three-dimensional cultures [83]. An MTT assay would not allow for the counting of cells, but it would allow for comparisons between different drug formulations. The development of cellular spheroids is advantageous for drug testing applications as tumors form dense cellular structures with necrotic cores similar to cellular spheroids.

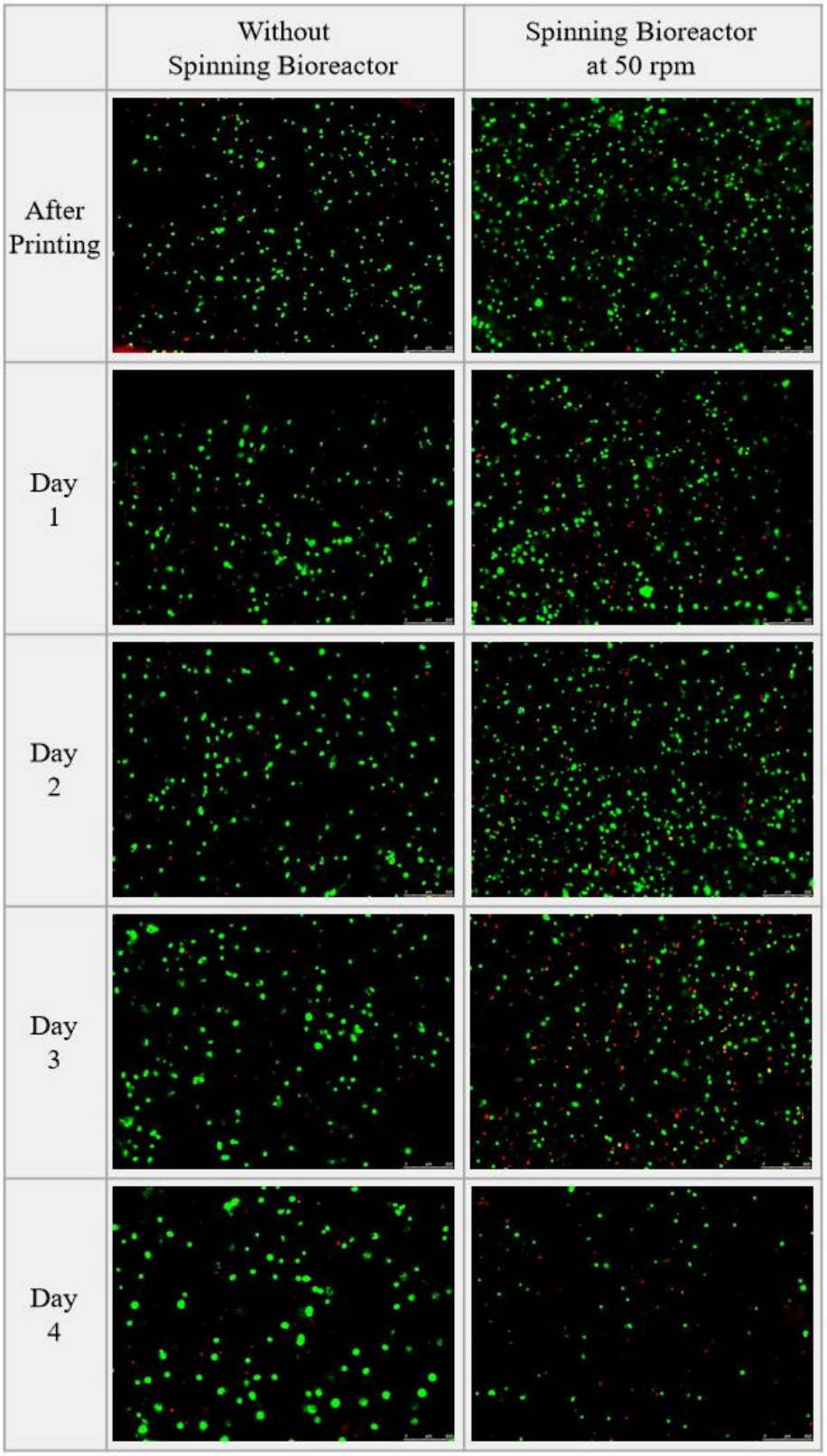


Figure 29. Fluorescence microscopy images of BxPC-3 cells in bioinks CF-CNC-Al with and without use of the spinning bioreactor.

# 5. CONCLUSIONS

## 5.1. Conclusions from Research Work

The goal of this project was to develop a system for pancreatic cancer drug testing that more closely mimicked an in vivo tumor microenvironment compared to current test methods. By bioprinting constructs containing pancreatic cancer cells, structures with a three-dimensional diffusion gradient and cellular interactions could be created, and a spinning bioreactor was designed to replicate vasculature and improve cell viability. When comparing bioink formulations, a CNC and alginate bioink provided better printability compared to a CMC and alginate bioink. Rheological testing showed that the CNCs provided more pronounced shear thinning than the CMC. This gives the CNC and alginate bioink a lower viscosity when it encounters high shear rates during extrusion through the print nozzle, which allows for smooth, consistent printing. Additionally, it displays a higher viscosity at low shear rates on the print bed, which prevents spreading and provides better shape fidelity. When analyzing a gelatin and alginate bioink, it was discovered that the gelatin dissolved out of the scaffolds during incubation, leading to poor structural stability for cell culture. Because of these reasons, the CNC and alginate bioink was chosen for further testing.

Cell viability in scaffolds of the CNC and alginate bioink ranged from nearly 80% after printing to around 60% after four days of culture. However, it was adversely affected by the use of the spinning bioreactor at 50 rpm. It was hypothesized that decreasing the rotational speed would prevent the bioreactor from disturbing the scaffolds while still increasing the rate of diffusion compared to stagnant conditions, thus improving cell viability and proliferation during the culture period. When testing bioreactor speeds of 10 and 20 rpm, mass cell death occurred during the printing process, making it difficult to compare the results to the 50-rpm testing.

Therefore, further optimizations on the printing procedure and spinning bioreactor speed should be performed. After addressing these issues, this system could be used for pancreatic cancer drug testing where it would better replicate the three-dimensional structure that is seen in in vivo tumor microenvironments.

### 5.2. Recommendations for Future Work

Although this system better matches the three-dimensional nature of a pancreatic cancer tumor than traditional two-dimensional cultures, further modifications would help to more closely replicate the in vivo environment. Optimizations such as increasing the bioink's stiffness and decreasing the nozzle size would improve the accuracy and resolution of printed constructs. Additionally, by altering the print geometry and specifically the raster width, lateral pores could be manufactured to provide better diffusion through the scaffold. To better replicate the environment of the pancreas, the stiffness of the scaffolds should be manipulated to match that of pancreatic tissue. This could be done by altering the material concentrations, crosslinking solution molarity, and crosslinking time, and nanoindentation could be used to verify the results. Lastly, further analysis of the scaffold morphology could be performed using scanning electron cryomicroscopy to look at the distribution of the different bioink components.

To maximize cell viability in the scaffolds, the rotational speed of the spinning bioreactor should be optimized to increase the rate of diffusion without disturbing the scaffolds. It is possible that slower bioreactor speeds than those tested here or non-constant stirring (i.e. stirring for only 15 minutes of each hour) would provide the desired increase in diffusion while minimizing scaffold disturbances. The mechanical properties of the scaffolds could also be evaluated over time to determine how the rotational speed affects them. Additionally, the spinning bioreactor could be compared to a perfusion bioreactor system, which more closely

replicates the flow of blood around a tumor microenvironment in vivo. Finally, testing should be performed to determine the optimal cell density in the bioink, as signaling cues from neighboring cells affect cell growth and proliferation.

After finalizing the system for use with cell lines, the system could be tested with cocultures of different cell types or with primary cell cultures to better replicate the in vivo tumor microenvironment. This is critical for optimal drug testing as previous studies have shown that drug sensitivity can vary between primary cultures and established cell lines [84]. Finally, the system could be used to test different free, encapsulated, and targeted drugs to evaluate the effectiveness and penetration of each, and the results should be compared to traditional two-dimensional cultures and three-dimensional spheroid cultures to determine the overall advantages and disadvantages of the system as a pancreatic cancer drug testing platform.

## REFERENCES


[1] F. Bray, J. Ferlay, I. Soerjomataram, R. L. Siegel, L. A. Torre, and A. Jemal, "Global cancer statistics 2018: GLOBOCAN estimates of incidence and mortality worldwide for 36 cancers in 185 countries," *CA: a cancer journal for clinicians,* vol. 68, no. 6, pp. 394-424, 2018.

[2] M. Hay, D. W. Thomas, J. L. Craighead, C. Economides, and J. Rosenthal, "Clinical development success rates for investigational drugs," *Nature biotechnology,* vol. 32, no. 1, p. 40, 2014.

[3] T. M. DesRochers, E. Palma, and D. L. Kaplan, "Tissue-engineered kidney disease models," *Advanced drug delivery reviews,* vol. 69, pp. 67-80, 2014.

[4] K. Chitcholtan, E. Asselin, S. Parent, P. H. Sykes, and J. J. Evans, "Differences in growth properties of endometrial cancer in three dimensional (3D) culture and 2D cell monolayer," *Experimental cell research,* vol. 319, no. 1, pp. 75-87, 2013.

[5] H. K. Dhiman, A. R. Ray, and A. K. Panda, "Three-dimensional chitosan scaffold-based MCF-7 cell culture for the determination of the cytotoxicity of tamoxifen," *Biomaterials,* vol. 26, no. 9, pp. 979-986, 2005.

[6] K. A. Fitzgerald, M. Malhotra, C. M. Curtin, F. J. O'brien, and C. M. O'driscoll, "Life in 3D is never flat: 3D models to optimise drug delivery," *Journal of controlled release,* vol. 215, pp. 39-54, 2015.

[7] S. Even-Ram and K. M. Yamada, "Cell migration in 3D matrix," *Current opinion in cell biology,* vol. 17, no. 5, pp. 524-532, 2005.

[8] G. Hamilton, "Multicellular spheroids as an in vitro tumor model," *Cancer letters,* vol. 131, no. 1, pp. 29-34, 1998.

[9] W. Mueller-Klieser, "Tumor biology and experimental therapeutics," *Critical reviews in oncology/hematology,* vol. 36, no. 2-3, pp. 123-139, 2000.

[10] G. M. Whitesides, "The origins and the future of microfluidics," *Nature,* vol. 442, no. 7101, p. 368, 2006.

[11] J. El-Ali, P. K. Sorger, and K. F. Jensen, "Cells on chips," *Nature,* vol. 442, no. 7101, p. 403, 2006.

[12] R. Daw and J. Finkelstein, "Lab on a chip," *Nature,* vol. 442, no. 7101, p. 367, 2006.

[13] S. Halldorsson, E. Lucumi, R. Gómez-Sjöberg, and R. M. Fleming, "Advantages and challenges of microfluidic cell culture in polydimethylsiloxane devices," *Biosensors and Bioelectronics,* vol. 63, pp. 218-231, 2015.

[14] S. Knowlton, S. Onal, C. H. Yu, J. J. Zhao, and S. Tasoglu, "Bioprinting for cancer research," *Trends in biotechnology,* vol. 33, no. 9, pp. 504-513, 2015.

[15] T. W. Ridky, J. M. Chow, D. J. Wong, and P. A. Khavari, "Invasive three-dimensional organotypic neoplasia from multiple normal human epithelia," *Nature medicine,* vol. 16, no. 12, p. 1450, 2010.

[16] S. Ghosh *et al.*, "Three-dimensional culture of melanoma cells profoundly affects gene expression profile: A high density oligonucleotide array study," *Journal of cellular physiology,* vol. 204, no. 2, pp. 522-531, 2005.

[17] C.-L. Li *et al.*, "Survival advantages of multicellular spheroids vs. monolayers of HepG2 cells in vitro," *Oncology reports,* vol. 20, no. 6, pp. 1465-1471, 2008.

[18] V. Chopra, T. Dinh, and E. Hannigan, "Three-dimensional endothelial-tumor epithelial cell interactions in human cervical cancers," *In Vitro Cellular & Developmental Biology-Animal,* vol. 33, no. 6, pp. 432-442, 1997.
[19] P. Friedl and K. Wolf, "Plasticity of cell migration: a multiscale tuning model," *The Journal of cell biology,* vol. 188, no. 1, pp. 11-19, 2010.
[20] D. Loessner, K. S. Stok, M. P. Lutolf, D. W. Hutmacher, J. A. Clements, and S. C. Rizzi, "Bioengineered 3D platform to explore cell–ECM interactions and drug resistance of epithelial ovarian cancer cells," *Biomaterials,* vol. 31, no. 32, pp. 8494-8506, 2010.
[21] Y. Zhao *et al.*, "Three-dimensional printing of Hela cells for cervical tumor model in vitro," *Biofabrication,* vol. 6, no. 3, p. 035001, 2014.
[22] X. Xu, C. R. Sabanayagam, D. A. Harrington, M. C. Farach-Carson, and X. Jia, "A hydrogel-based tumor model for the evaluation of nanoparticle-based cancer therapeutics," *Biomaterials,* vol. 35, no. 10, pp. 3319-3330, 2014.
[23] A. Frankel, R. Buckman, and R. S. Kerbel, "Abrogation of taxol-induced G2-M arrest and apoptosis in human ovarian cancer cells grown as multicellular tumor spheroids," *Cancer research,* vol. 57, no. 12, pp. 2388-2393, 1997.
[24] L. W. Dunne *et al.*, "Human decellularized adipose tissue scaffold as a model for breast cancer cell growth and drug treatments," *Biomaterials,* vol. 35, no. 18, pp. 4940-4949, 2014.
[25] I. Serebriiskii, R. Castelló-Cros, A. Lamb, E. A. Golemis, and E. Cukierman, "Fibroblast-derived 3D matrix differentially regulates the growth and drug-responsiveness of human cancer cells," *Matrix Biology,* vol. 27, no. 6, pp. 573-585, 2008.
[26] Y.-J. Kim, H.-I. Bae, O. K. Kwon, and M.-S. Choi, "Three-dimensional gastric cancer cell culture using nanofiber scaffold for chemosensitivity test," *International journal of biological macromolecules,* vol. 45, no. 1, pp. 65-71, 2009.
[27] L. A. Gurski, A. K. Jha, C. Zhang, X. Jia, and M. C. Farach-Carson, "Hyaluronic acid-based hydrogels as 3D matrices for in vitro evaluation of chemotherapeutic drugs using poorly adherent prostate cancer cells," *Biomaterials,* vol. 30, no. 30, pp. 6076-6085, 2009.
[28] M. S. Molla, D. R. Katti, and K. S. Katti, "In vitro design of mesenchymal to epithelial transition of prostate cancer metastasis using 3D nanoclay bone-mimetic scaffolds," *Journal of tissue engineering and regenerative medicine,* vol. 12, no. 3, pp. 727-737, 2018.
[29] K. A. Fitzgerald *et al.*, "The use of collagen-based scaffolds to simulate prostate cancer bone metastases with potential for evaluating delivery of nanoparticulate gene therapeutics," *Biomaterials,* vol. 66, pp. 53-66, 2015.
[30] C. Fischbach *et al.*, "Engineering tumors with 3D scaffolds," *Nature methods,* vol. 4, no. 10, p. 855, 2007.
[31] R. Nigam and B. Mahanta, "An overview of various biomimetic scaffolds: Challenges and applications in tissue engineering," *Journal of Tissue Science & Engineering,* vol. 5, no. 2, p. 1, 2014.
[32] M. R. Junttila and F. J. de Sauvage, "Influence of tumour micro-environment heterogeneity on therapeutic response," *Nature,* vol. 501, no. 7467, p. 346, 2013.
[33] U. S. D. o. H. a. H. Services. "Organ Procurement and Transplantation Network." https://optn.transplant.hrsa.gov/ (accessed Nov 26, 2018).

[34] M. Hospodiuk, M. Dey, D. Sosnoski, and I. T. Ozbolat, "The bioink: A comprehensive review on bioprintable materials," *Biotechnology advances,* vol. 35, no. 2, pp. 217-239, 2017.
[35] S. V. Murphy and A. Atala, "3D bioprinting of tissues and organs," *Nature biotechnology,* vol. 32, no. 8, p. 773, 2014.
[36] A. W. Feinberg and J. S. Miller, "Progress in three-dimensional bioprinting," *MRS Bulletin,* vol. 42, no. 8, pp. 557-562, 2017.
[37] Y. He, F. Yang, H. Zhao, Q. Gao, B. Xia, and J. Fu, "Research on the printability of hydrogels in 3D bioprinting," *Scientific reports,* vol. 6, p. 29977, 2016.
[38] J. Li, M. Chen, X. Fan, and H. Zhou, "Recent advances in bioprinting techniques: approaches, applications and future prospects," *Journal of translational medicine,* vol. 14, no. 1, p. 271, 2016.
[39] S. Jana and A. Lerman, "Bioprinting a cardiac valve," *Biotechnology advances,* vol. 33, no. 8, pp. 1503-1521, 2015.
[40] F. P. Melchels, J. Feijen, and D. W. Grijpma, "A review on stereolithography and its applications in biomedical engineering," *Biomaterials,* vol. 31, no. 24, pp. 6121-6130, 2010.
[41] A. Panwar and L. P. Tan, "Current status of bioinks for micro-extrusion-based 3D bioprinting," *Molecules,* vol. 21, no. 6, p. 685, 2016.
[42] K. Nair *et al.*, "Characterization of cell viability during bioprinting processes," *Biotechnology Journal: Healthcare Nutrition Technology,* vol. 4, no. 8, pp. 1168-1177, 2009.
[43] D. F. Duarte Campos *et al.*, "The stiffness and structure of three-dimensional printed hydrogels direct the differentiation of mesenchymal stromal cells toward adipogenic and osteogenic lineages," *Tissue Engineering Part A,* vol. 21, no. 3-4, pp. 740-756, 2014.
[44] A. Skardal and A. Atala, "Biomaterials for integration with 3-D bioprinting," *Annals of biomedical engineering,* vol. 43, no. 3, pp. 730-746, 2015.
[45] P. Soman *et al.*, "Cancer cell migration within 3D layer-by-layer microfabricated photocrosslinked PEG scaffolds with tunable stiffness," *Biomaterials,* vol. 33, no. 29, pp. 7064-7070, 2012.
[46] J. Zhu and R. E. Marchant, "Design properties of hydrogel tissue-engineering scaffolds," *Expert review of medical devices,* vol. 8, no. 5, pp. 607-626, 2011.
[47] G. Gao, T. Yonezawa, K. Hubbell, G. Dai, and X. Cui, "Inkjet-bioprinted acrylated peptides and PEG hydrogel with human mesenchymal stem cells promote robust bone and cartilage formation with minimal printhead clogging," *Biotechnology journal,* vol. 10, no. 10, pp. 1568-1577, 2015.
[48] T. Billiet, E. Gevaert, T. De Schryver, M. Cornelissen, and P. Dubruel, "The 3D printing of gelatin methacrylamide cell-laden tissue-engineered constructs with high cell viability," *Biomaterials,* vol. 35, no. 1, pp. 49-62, 2014.
[49] M. Müller, J. Becher, M. Schnabelrauch, and M. Zenobi-Wong, "Nanostructured Pluronic hydrogels as bioinks for 3D bioprinting," *Biofabrication,* vol. 7, no. 3, p. 035006, 2015.
[50] K. Markstedt, A. Mantas, I. Tournier, H. c. Martínez Ávila, D. Hägg, and P. Gatenholm, "3D bioprinting human chondrocytes with nanocellulose–alginate bioink for cartilage tissue engineering applications," *Biomacromolecules,* vol. 16, no. 5, pp. 1489-1496, 2015.

[51] Y. Wu, Z. Y. W. Lin, A. C. Wenger, K. C. Tam, and X. S. Tang, "3D bioprinting of liver-mimetic construct with alginate/cellulose nanocrystal hybrid bioink," *Bioprinting,* vol. 9, pp. 1-6, 2018.
[52] J. Jia *et al.*, "Engineering alginate as bioink for bioprinting," *Acta biomaterialia,* vol. 10, no. 10, pp. 4323-4331, 2014.
[53] I. Henriksson, P. Gatenholm, and D. Hägg, "Increased lipid accumulation and adipogenic gene expression of adipocytes in 3D bioprinted nanocellulose scaffolds," *Biofabrication,* vol. 9, no. 1, p. 015022, 2017.
[54] P. O. Staff, "Correction: chondrogenesis of infrapatellar fat pad derived adipose stem cells in 3D printed chitosan scaffold," *PloS one,* vol. 9, no. 7, p. e102638, 2014.
[55] C. M. Smith *et al.*, "Three-dimensional bioassembly tool for generating viable tissue-engineered constructs," *Tissue engineering,* vol. 10, no. 9-10, pp. 1566-1576, 2004.
[56] F. Pati *et al.*, "Printing three-dimensional tissue analogues with decellularized extracellular matrix bioink," *Nature communications,* vol. 5, p. 3935, 2014.
[57] M. B. Dainiak *et al.*, "Gelatin–fibrinogen cryogel dermal matrices for wound repair: preparation, optimisation and in vitro study," *Biomaterials,* vol. 31, no. 1, pp. 67-76, 2010.
[58] K. Schacht, T. Jüngst, M. Schweinlin, A. Ewald, J. Groll, and T. Scheibel, "Biofabrication of cell-loaded 3D spider silk constructs," *Angewandte Chemie International Edition,* vol. 54, no. 9, pp. 2816-2820, 2015.
[59] A. Homayouni, M. R. Ehsani, A. Azizi, M. S. Yarmand, and H. RAZAVI, "Effect of lecithin and calcium chloride solution on the microencapsulation process yield of calcium alginate beads," 2007.
[60] J.-H. Shim, J.-S. Lee, J. Y. Kim, and D.-W. Cho, "Bioprinting of a mechanically enhanced three-dimensional dual cell-laden construct for osteochondral tissue engineering using a multi-head tissue/organ building system," *Journal of Micromechanics and Microengineering,* vol. 22, no. 8, p. 085014, 2012.
[61] J. George and S. Sabapathi, "Cellulose nanocrystals: synthesis, functional properties, and applications," *Nanotechnology, science and applications,* vol. 8, p. 45, 2015.
[62] C. C. Piras, S. Fernández-Prieto, and W. M. De Borggraeve, "Nanocellulosic materials as bioinks for 3D bioprinting," *Biomaterials science,* vol. 5, no. 10, pp. 1988-1992, 2017.
[63] A. O. Elzoghby, "Gelatin-based nanoparticles as drug and gene delivery systems: reviewing three decades of research," *Journal of Controlled Release,* vol. 172, no. 3, pp. 1075-1091, 2013.
[64] V. Lee *et al.*, "Design and fabrication of human skin by three-dimensional bioprinting," *Tissue Engineering Part C: Methods,* vol. 20, no. 6, pp. 473-484, 2013.
[65] X. Cui, K. Breitenkamp, M. Finn, M. Lotz, and D. D. D'Lima, "Direct human cartilage repair using three-dimensional bioprinting technology," *Tissue Engineering Part A,* vol. 18, no. 11-12, pp. 1304-1312, 2012.
[66] J. S. Miller *et al.*, "Rapid casting of patterned vascular networks for perfusable engineered three-dimensional tissues," *Nature materials,* vol. 11, no. 9, p. 768, 2012.
[67] S. Bose, S. Vahabzadeh, and A. Bandyopadhyay, "Bone tissue engineering using 3D printing," *Materials today,* vol. 16, no. 12, pp. 496-504, 2013.
[68] M. S. Mannoor *et al.*, "3D printed bionic ears," *Nano letters,* vol. 13, no. 6, pp. 2634-2639, 2013.

[69] J. W. Chang *et al.*, "Tissue-engineered tracheal reconstruction using three-dimensionally printed artificial tracheal graft: preliminary report," *Artificial organs,* vol. 38, no. 6, pp. E95-E105, 2014.
[70] A. Atala, S. B. Bauer, S. Soker, J. J. Yoo, and A. B. Retik, "Tissue-engineered autologous bladders for patients needing cystoplasty," *The lancet,* vol. 367, no. 9518, pp. 1241-1246, 2006.
[71] M. Lovett, K. Lee, A. Edwards, and D. L. Kaplan, "Vascularization strategies for tissue engineering," *Tissue Engineering Part B: Reviews,* vol. 15, no. 3, pp. 353-370, 2009.
[72] M. S. Hahn, M. K. McHale, E. Wang, R. H. Schmedlen, and J. L. West, "Physiologic pulsatile flow bioreactor conditioning of poly (ethylene glycol)-based tissue engineered vascular grafts," *Annals of biomedical engineering,* vol. 35, no. 2, pp. 190-200, 2007.
[73] D. G. Moon, G. Christ, J. D. Stitzel, A. Atala, and J. J. Yoo, "Cyclic mechanical preconditioning improves engineered muscle contraction," *Tissue Engineering Part A,* vol. 14, no. 4, pp. 473-482, 2008.
[74] N. Charbe, P. A. McCarron, and M. M. Tambuwala, "Three-dimensional bio-printing: A new frontier in oncology research," *World journal of clinical oncology,* vol. 8, no. 1, p. 21, 2017.
[75] "Rheology Solutions," *Determining the Linear Viscoelastic Region in Polymers,*
[76] X. Qian, F. Jacob, M. M. Song, H. N. Nguyen, H. Song, and G.-l. Ming, "Generation of human brain region–specific organoids using a miniaturized spinning bioreactor," *Nature protocols,* vol. 13, no. 3, p. 565, 2018.
[77] P. S. Thayer, L. S. Orrhult, and H. Martínez, "Bioprinting of Cartilage and Skin Tissue Analogs Utilizing a Novel Passive Mixing Unit Technique for Bioink Precellularization," *Journal of visualized experiments: JoVE,* no. 131, 2018.
[78] A. Habib, V. Sathish, S. Mallik, and B. Khoda, "3D printability of alginate-carboxymethyl cellulose hydrogel," *Materials,* vol. 11, no. 3, p. 454, 2018.
[79] A. Castellan, R. Ruggiero, E. Frollini, L. A. Ramos, and C. Chirat, "Studies on fluorescence of cellulosics," *Holzforschung,* vol. 61, no. 5, pp. 504-508, 2007.
[80] N. Cao, X. Chen, and D. Schreyer, "Influence of calcium ions on cell survival and proliferation in the context of an alginate hydrogel," *ISRN Chemical Engineering,* vol. 2012, 2012.
[81] M. S. Reid, M. Villalobos, and E. D. Cranston, "Benchmarking cellulose nanocrystals: from the laboratory to industrial production," *Langmuir,* vol. 33, no. 7, pp. 1583-1598, 2016.
[82] C. R. Kruse *et al.*, "The effect of pH on cell viability, cell migration, cell proliferation, wound closure, and wound reepithelialization: In vitro and in vivo study," *Wound Repair and Regeneration,* vol. 25, no. 2, pp. 260-269, 2017.
[83] C. Intini *et al.*, "3D-printed chitosan-based scaffolds: An in vitro study of human skin cell growth and an in-vivo wound healing evaluation in experimental diabetes in rats," *Carbohydrate polymers,* vol. 199, pp. 593-602, 2018.
[84] Z. Xu *et al.*, "Application of a microfluidic chip-based 3D co-culture to test drug sensitivity for individualized treatment of lung cancer," *Biomaterials,* vol. 34, no. 16, pp. 4109-4117, 2013.